Research article JHEP|Reports

# Liver fibrosis and CD206$^{+}$ macrophage accumulation are suppressed by anti-GM-CSF therapy


## Authors

Alfonso Tan-Garcia, Fritz Lai, Joe Poh Sheng Yeong, Sergio E. Irac, Pei Y. Ng, Rasha Msallam, Jeffrey Chun Tatt Lim, Lu-En Wai, Christine Y.L. Tham, Su P. Choo, Tony Lim, Dan Y. Young, Roberta D'Ambrosio, Elisabetta Degasperi, Riccardo Perbellini, Evan Newell, Nina Le Bert, Florent Ginhoux, Antonio Bertoletti, Qingfeng Chen, Charles-Antoine Dutertre

## Correspondence

charles_dutertre@immunol.a-star.edu.sg (C.-A. Dutertre), qchen@imcb.a-star.edu.sg (Q. Chen).


## Graphical abstract

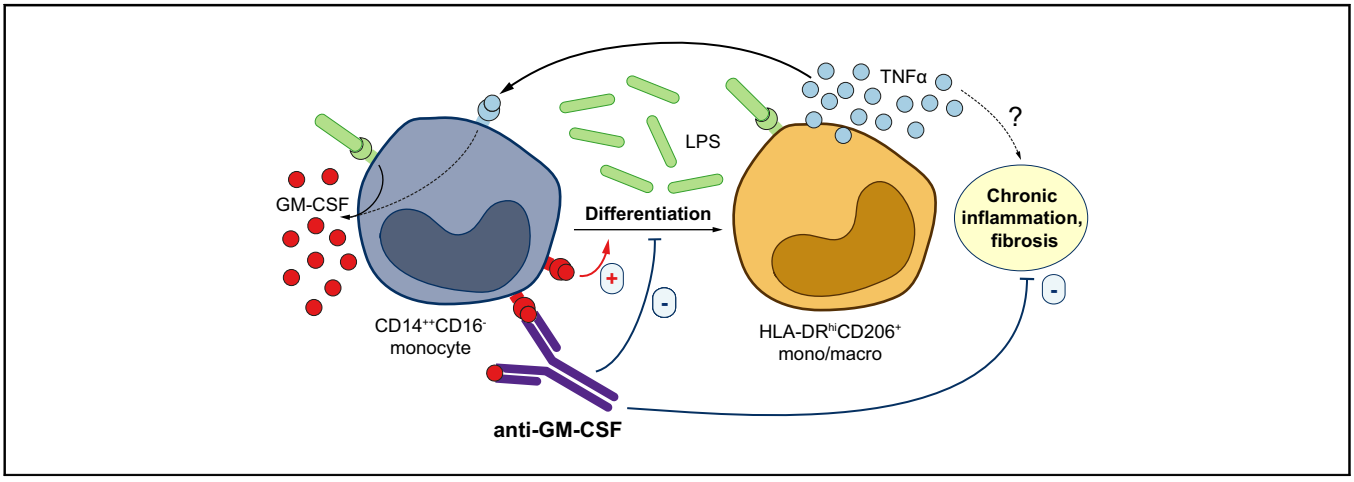


## Highlights

- GM-CSF and TNFα producing CD206$^{+}$ macrophages accumulate in human fibrotic liver
- Serum GM-CSF is increased in HCV$^{+}$ patients with higher liver fibrosis
- GM-CSF drives monocyte to CD206$^{+}$ macrophage conversion
- Anti-GM-CSF therapy suppresses liver fibrosis and CD206$^{+}$ macrophage accumulation

## Lay summary

Liver fibrosis is a major driver of liver disease progression. Herein, we have shown that granulocyte-macrophage colony-stimulating factor (GM-CSF) plays an important role in the development of liver fibrosis. Our findings support the use of anti-GM-CSF neutralising antibodies for the management of patients with chronic liver disease resulting from both viral and non-viral causes.

https://doi.org/10.1016/j.jhepr.2019.11.006

Research article

JHEP|Reports

# Liver fibrosis and CD206$^+$ macrophage accumulation are suppressed by anti-GM-CSF therapy

Alfonso Tan-Garcia,[1,‡] Fritz Lai,[2,‡] Joe Poh Sheng Yeong,[3] Sergio E. Irac,[1] Pei Y. Ng,[4] Rasha Msallam,[4] Jeffrey Chun Tatt Lim,[3] Lu-En Wai,[1] Christine Y.L. Tham,[1] Su P. Choo,[5] Tony Lim,[3] Dan Y. Young,[6] Roberta D'Ambrosio,[7] Elisabetta Degasperi,[7] Riccardo Perbellini,[7] Evan Newell,[4,8] Nina Le Bert,[1] Florent Ginhoux,[4] Antonio Bertoletti,[1,4] Qingfeng Chen,[2,9,*] Charles-Antoine Dutertre[1,4,*]

[1]*Program in Emerging Infectious Diseases, Duke-NUS Medical School, 8 College Road, Singapore 169857, Singapore;* [2]*Humanised Mouse Unit, Institute of Molecular and Cell Biology, A*STAR, 61 Biopolis Drive, Singapore 138673, Singapore;* [3]*Department of Anatomical Pathology, Singapore General Hospital, Singapore;* [4]*Singapore Immunology Network, A*STAR, 8A Biomedical Grove, Immunos Building, Level 4, Singapore 138648, Singapore;* [5]*Department of Medical Oncology, National Cancer Centre, Singapore;* [6]*Department of Medicine, Yong Loo Lin School of Medicine, National University of Singapore, Singapore; Division of Gastroenterology and Hepatology, National University Hospital, National University Health System, Singapore;* [7]*CRC "A.M. e A. Migliavacca" Center for the Study of Liver Disease, Division of Gastroenterology and Hepatology, Fondazione IRCCS Ca' Granda - Ospedale Maggiore Policlinico, Milan, Italy;* [8]*Fred Hutch Cancer Research Center, Vaccine and Infectious Disease Division, Seattle, WA, USA;* [9]*Department of Physiology, Yong Loo Lin School of Medicine, National University of Singapore, 119228, Singapore*

JHEP Reports **2020.** https://doi.org/10.1016/j.jhepr.2019.11.006

**Background & Aims:** Chronic liver inflammation leads to fibrosis and cirrhosis and is associated with an accumulation of intrahepatic TNFα-secreting CD206$^+$ macrophages, which may participate in maintaining chronic liver disease in a GM-CSF-dependent manner. We aimed to elucidate the exact role of GM-CSF in the development and progression of chronic liver disease.

**Methods:** Liver immunohistochemistry and serum quantification were performed in patients with viral and non-viral-related liver disease to compare CD206$^+$ monocyte/macrophages, fibrosis and GM-CSF. This was followed by functional validations *in vitro* and *in vivo* in humanised mice.

**Results:** Using multiplex immunofluorescence and histo-cytometry, we show that highly fibrotic livers had a greater density of CD206$^+$ macrophages that produced more TNFα and GM-CSF in the non-tumour liver regions of patients with hepatocellular carcinoma (n = 47), independent of aetiology. In addition, the absolute number of CD206$^+$ macrophages strongly correlated with the absolute number of GM-CSF-producing macrophages. In non-HCC chronic HCV$^+$ patients (n = 40), circulating GM-CSF levels were also increased in proportion to the degree of liver fibrosis and serum viral titres. We then demonstrated *in vitro* that monocytes converted to TNFα-producing CD206$^+$ macrophage-like cells in response to bacterial products (lipopolysaccharide) in a GM-CSF-dependent manner, confirming the *in vivo* normalisation of serum GM-CSF concentration following oral antibiotic treatment observed in HBV-infected humanised mice. Finally, anti-GM-CSF neutralising antibody treatment reduced intrahepatic CD206$^+$ macrophage accumulation and abolished liver fibrosis in HBV-infected humanised mice.

**Conclusions:** While the direct involvement of CD206$^+$ macrophages in liver fibrosis remains to be demonstrated, these findings show that GM-CSF may play a central role in liver fibrosis and could guide the development of anti-GM-CSF antibody-based therapy for the management of patients with chronic liver disease.



Keywords: Intrahepatic macrophages; GM-CSF; CD206$^+$ macrophages; fibrosis; anti-GM-CSF neutralizing antibody; HCV; NASH.

*Received 22 August 2019; received in revised form 18 November 2019; accepted 20 November 2019; available online XXX*

‡ Co-first authors (Equal contribution).

* Corresponding authors. Addresses: Program in Emerging Infectious Diseases, Duke-NUS Medical School, 8 College Road, Singapore 169857, Singapore and Singapore Immunology Network, A*STAR, 8A Biomedical Grove, Immunos Building, Level 4, Singapore 138648, Singapore; Tel.: (+65) 84223021 (C.-A. Dutertre), or Humanised Mouse Unit, Institute of Molecular and Cell Biology, A*STAR, 61 Biopolis Drive, Singapore 138673, Singapore; Tel.: (+65) 6586 9873 (Q. Chen).

*E-mail addresses*: charles_dutertre@immunol.a-star.edu.sg (C.-A. Dutertre), qchen@imcb.a-star.edu.sg (Q. Chen).

## Introduction

Liver inflammation is pivotal to the progression of chronic liver disease to end-stage complications such as fibrosis, cirrhosis and hepatocellular carcinoma (HCC).[1] The identification of proinflammatory CD14$^+$HLA-DR$^{hi}$CD206$^+$ macrophages resistant to endotoxin tolerance – in a granulocyte-macrophage colony-stimulating factor (GM-CSF)-dependent manner – within the liver of patients with advanced chronic viral hepatitis[2] demonstrated the importance of the intrahepatic myeloid compartment in chronic liver inflammation. However, the mechanisms that mediate the accumulation of intrahepatic CD14$^+$HLA-DR$^{hi}$CD206$^+$ macrophages remain poorly defined.

GM-CSF is part of the CSF superfamily of growth factors which are required for the development of monocytes, macrophages, dendritic cells (DCs) and granulocytes from myeloid precursors.[3] GM-CSF is a monomeric glycoprotein that is secreted by both haematopoietic and non-haematopoietic cells upon stimulation.[4,5] Unlike granulocyte colony-stimulating factor and macrophage colony-stimulating factor, which are indispensable for steady state myelopoiesis,[6–8] GM-CSF is increasingly recognised as a central mediator of immune activation and inflammation.[3,9,10] Helper T cell ($T_H$)-derived GM-CSF has been demonstrated to induce an inflammatory phenotype in central nervous system-infiltrating myeloid cells leading to demyelination and neurological deficits in experimental autoimmune encephalitis[11–15] and GM-CSF-overexpressing transgenic mouse models.[16] Consistent with the observations in animal models, GM-CSF has also been implicated in human autoimmune diseases. Elevated concentrations of GM-CSF have been detected in the cerebrospinal fluid of patients with multiple sclerosis (MS), providing further evidence of the involvement of GM-CSF in neuroinflammation.[17] Elevated concentrations of GM-CSF have been detected in the synovial fluid of patients with rheumatoid arthritis (RA)[18] and administration of recombinant GM-CSF in these patients exacerbates disease activity.[19]

Despite the overwhelming evidence supporting its role in autoimmune diseases, GM-CSF has not been implicated in chronic liver disease. In this study, using multiplex immunofluorescent histology and histo-cytometric analyses of liver tissues from 47 patients with HCC secondary to viral and non-viral aetiologies, we demonstrated that the intrahepatic expression of GM-CSF and $CD206^+$ macrophage density correlated with the degree of liver fibrosis. We also showed that serum GM-CSF concentration was elevated in patients with chronic HCV who had higher viral titres and more advanced liver fibrosis, as well as in patients with non-alcoholic steatohepatitis (NASH) who had more advanced liver fibrosis. Serum GM-CSF was also increased in HBV-infected humanised mice in direct correlation with intrahepatic $CD206^+$ macrophage frequency and it was normalised following oral antibiotic treatment. We next demonstrated that microbial products (lipopolysaccharide [LPS]) drove the differentiation of monocytes into $CD206^+$ macrophages in a GM-CSF-dependent manner. Importantly, both prophylactic and therapeutic treatment of HBV-infected humanised mice using a neutralising anti-GM-CSF antibody reduced the number of $CD206^+$ macrophages and abolished liver fibrosis. These findings highlight, for the first time, that GM-CSF is a central mediator of liver inflammation and fibrosis, providing evidence of novel therapeutic approaches for the management of patients with chronic liver disease.

## Materials and methods

### Human blood and serum samples

Peripheral blood from healthy donors was collected by venepuncture with heparin anti-coagulation or post-apheresis with citrate anti-coagulation (Health Sciences Authority, Singapore) and peripheral blood mononuclear cells (PBMCs) were freshly purified on a Ficoll density gradient. Sera was collected from 7 healthy donors, from 40 patients with HCV before and after direct-acting antiviral (DAA) therapy at a single tertiary centre in Milan, Italy (Table 2), and from 18 patients with NASH. Patients with HCV were treated between 2014 and 2017 with available DAA regimens, according to International recommendations. All patients with HCV underwent pre- and post-treatment (12 weeks) clinical assessments, which included HCV RNA, aminotransferases and platelet values. Fibrosis stage was assessed non-invasively, through transient elastography; cirrhosis (F4) was identified by a liver stiffness measurement (LSM) >11.9 kPa. A sustained virological response (SVR) was defined as HCV RNA undetectability 12 weeks after the end of treatment.

### Multiplex immunohistochemistry and confocal microscopy

Multiplex immunohistochemistry was performed using an Opal Multiplex flHC kit (PerkinElmer, Waltham, MA, USA) and a Leica Bond Max autostainer (Leica Biosystems Melbourne, Australia). Deparaffinised and rehydrated formalin-fixed paraffin-embedded (FFPE) tissue sections were subjected to heat-induced epitope retrieval (HIER; Leica Biosystems Newcastle, UK) and incubated with a primary antibody for GM-CSF (Novus Biologicals LLC, Centennial, CO, USA), CD14 (Abcam Plc, Cambridge, UK), CD206 (Bio-Rad Laboratories Inc, Hercules, CA, USA) or CD68 (Dako Denmark A/S). Secondary antibodies (Leica Biosystems Newcastle, UK) were then applied, followed by fluorophore-conjugated tyramide signal amplification (TSA) buffer (PerkinElmer, Waltham, MA, USA): Opal 520 or Opal 570 (FITC and Cy3 equivalent respectively). HIER and antibody incubation steps were repeated for a second primary antibody and TSA. Spectral DAPI (PerkinElmer, Waltham, MA, USA) was used as a nuclear counterstain prior to coverslipping in antifade mountant (Life Technologies Corp, Eugene, OR, USA). The antibodies used were the same as for tissue microarray (TMA) staining (described below, see Table 1). Confocal images were acquired using an FV-1000 confocal system combined to an inverted Olympus IX81 microscope (40x objective) and analysed using the Image J 1.51m9 software.

### Patients and tumours used for the histo-cytometry analyses

A total of 47 archival FFPE adjacent normal liver specimens from patients diagnosed with hepatocellular carcinoma between January 2001 and December 2011 at the Department of Anatomical Pathology, Division of Pathology, Singapore General Hospital, were analysed (Table 1). All samples were obtained before patients underwent chemo- or radiotherapy. Clinicopathological parameters, including patient age, tumour size, histologic growth pattern, grade and subtype, associated ductal carcinoma *in situ*, lymphovascular invasion and axillary lymph node status, are reviewed. Tumours were typed, staged and graded according to the World Health Organization, American Society of Clinical Oncology-College of American Pathologists (ASCO-CAP) guidelines.[20] Ishak fibrosis score[21,22] was adopted to evaluate the fibrosis status of the non-neoplastic liver; these scores are documented in the pathological diagnostic reports. The Centralized Institutional Review Board of SingHealth provided ethical approval for the use of patient materials in this study (CIRB ref: 2009/907/B).

### Tissue microarray construction

Non-neoplastic liver regions were selected for TMA construction based on pathological assessment which identified samples where 100% of the sample area was non-neoplastic liver tissue. For each sample, 2 or 3 representative tumour cores of 1 mm diameter were transferred from donor FFPE tissue blocks to recipient TMA blocks using an MTA-1 Manual Tissue Arrayer

**Table 1. Clinical data of patients with HCC analysed by multiplex histology.**

| TMA Block No. | HBV | HCV | Fibrosis (Y/N) | Fibrosis stage (Ishak/6) | Cirrhosis (Y/N) | Steatosis/fatty change (Y/N) | [a]Age | Gender | Ethnic group |
|---|---|---|---|---|---|---|---|---|---|
| TMA4A-03 | n.a. | n.a. | N | 0 | N | No | 33 | Female | Others |
| TMA3B-06 | n.a. | n.a. | N | 0 | N | n.a. | 70 | Male | Chinese |
| TMA3B-03 | n.a. | n.a. | N | 0 | - | n.a. | 47 | Male | Chinese |
| TMA5C-10 | Negative | Negative | N | 0 | N | Yes | 70 | Male | Others |
| TMA5C-11 | Negative | Negative | N | 0 | N | n.a. | 71 | Male | Chinese |
| TMA5C-16 | Negative | Negative | N | 0 | N | n.a. | 57 | Male | Chinese |
| TMA7B-11 | Positive | n.a. | N | 0 | N | n.a. | 49 | Male | Chinese |
| TMA4A-16 | Positive | Negative | N | 0 | – | n.a. | 72 | Female | Chinese |
| TMA3B-05 | Positive | Negative | N | 0 | N | Yes | 75 | Male | Chinese |
| TMA4A-10 | Negative | Positive | Y | 2 | N | Yes | 66 | Female | Chinese |
| TMA3B-14 | n.a. | Negative | Y | 3 | N | Yes | 73 | Male | Chinese |
| TMA4A-24 | Positive | Negative | Y | 3 | N | Yes | 44 | Male | Chinese |
| TMA5C-18 | Positive | Negative | Y | 5 | Y | Yes | 48 | Female | Chinese |
| TMA5C-08 | Positive | Negative | Y | 5 | Y | Yes | 69 | Male | Chinese |
| TMA4A-09 | n.a. | n.a. | Y | 6 | Y | No | 48 | Male | Chinese |
| TMA4A-14 | n.a. | n.a. | Y | 6 | Y | Yes | 68 | Male | Chinese |
| TMA3B-21 | n.a. | Positive | Y | 6 | Y | n.a. | 71 | Male | Others |
| TMA5C-01 | Negative | n.a. | Y | 6 | Y | Yes | 56 | Male | Chinese |
| TMA4A-07 | Negative | Negative | Y | 6 | Y | n.a. | 78 | Female | Indian |
| TMA4A-04 | Negative | Negative | Y | 6 | Y | n.a. | 70 | Male | Chinese |
| TMA4A-12 | Negative | Negative | Y | 6 | Y | n.a. | 79 | Female | Chinese |
| TMA3B-13 | Negative | Negative | Y | 6 | Y | Yes | 64 | Male | Chinese |
| TMA3B-09 | Negative | Negative | Y | 6 | Y | n.a. | 57 | Male | Chinese |
| TMA3B-10 | Negative | Negative | Y | 6 | Y | n.a. | 67 | Male | Others |
| TMA3B-19 | Negative | Negative | Y | 6 | Y | n.a. | 68 | Male | Chinese |
| TMA3B-07 | Negative | Negative | Y | 6 | Y | Yes | 70 | Male | Chinese |
| TMA3B-24 | Negative | Negative | Y | 6 | Y | n.a. | 66 | Male | Chinese |
| TMA4A-18 | Negative | Positive | Y | 6 | Y | n.a. | 70 | Female | Others |
| TMA4A-11 | Negative | Positive | Y | 6 | Y | n.a. | 66 | Male | Chinese |
| TMA4A-08 | Positive | n.a. | Y | 6 | Y | n.a. | 68 | Female | Chinese |
| TMA5C-14 | Positive | n.a. | Y | 6 | Y | n.a. | 47 | Female | Chinese |
| TMA5C-03 | Positive | n.a. | Y | 6 | Y | n.a. | 65 | Male | Chinese |
| TMA4A-19 | Positive | Negative | Y | 6 | Y | Yes | 64 | Male | Chinese |
| TMA5C-13 | Positive | Negative | Y | 6 | Y | n.a. | 57 | Male | Chinese |
| TMA5C-12 | Positive | Negative | Y | 6 | Y | n.a. | 74 | Male | Chinese |
| TMA3B-01 | Positive | Negative | Y | 6 | Y | n.a. | 64 | Male | Chinese |
| TMA3B-15 | Positive | Negative | Y | 6 | Y | n.a. | 47 | Male | Chinese |
| TMA3B-20 | Positive | Negative | Y | 6 | Y | Yes | 68 | Female | Chinese |
| TMA3B-12 | Positive | Negative | Y | 6 | Y | n.a. | 64 | Female | Chinese |
| TMA3B-17 | Positive | n.a. | Y | 1-2 | N | n.a. | 45 | Male | Chinese |
| TMA4A-02 | Positive | Negative | Y | 1-2 | N | Yes | 53 | Male | Chinese |
| TMA5C-05 | Positive | Negative | Y | 1-2 | N | Yes | 49 | Female | Chinese |
| TMA5C-22 | Positive | Negative | Y | 1-2 | N | No | 56 | Male | Chinese |
| TMA4A-05 | Positive | Negative | Y | 3-4 | N | n.a. | 57 | Male | Chinese |
| TMA5C-04 | n.a. | n.a. | Y | 5-6 | Y | Yes | 80 | Female | Chinese |
| TMA3B-11 | Positive | n.a. | Y | 5-6 | Y | Yes | 64 | Male | Chinese |
| TMA3B-08 | Positive | Negative | Y | 5-6 | Y | Yes | 64 | Male | Chinese |

[a] Age when operated. HCC, hepatocellular carcinoma.

(Beecher Instruments, Inc., Sun Prairie, WI, USA). TMAs were constructed as previously described.[23]

### Multiplex immunofluorescence

Multiplex immunofluorescence was performed using an Opal Multiplex flHC kit (PerkinElmer, Inc., Waltham, MA, USA), on FFPE tissue sections processed according to the standard immunohistochemistry protocol. Slides were incubated with primary antibodies against cytokeratin (CK), CD14, CD206, GM-CSF, and TNFα (as presented in Table S1), followed by appropriate secondary antibodies, before application of the fluorophore-conjugated tyramides signal amplification buffer (PerkinElmer, Inc., Waltham, MA, USA). DAPI was used as a nuclear counterstain, and images were acquired using a Vectra 3 pathology imaging system microscope (PerkinElmer, Inc.) and analysed using inForm version 2.3 software (PerkinElmer, Inc.). Mean intensities of each stain were determined in the nucleus, cytoplasm and membrane of individual cells delineated in each image. For DAPI, nucleus quantification was used but for the other stainings, cytoplasmic quantification was used rather than membrane quantification to limit contaminating signals coming from neighbouring cells. Data were next analysed by histo-cytometry using the FlowJo software (Tree Star). Merged images of CD14 and GM-CSF co-stainings were obtained using the Image J 1.51m9 software.

### Flow cytometric analyses

PBMCs were stained as previously described[24] and analysed using a LSRFortessa (BD Biosciences). Dead cells were excluded using Live/Dead Blue dye (Invitrogen). For intracellular cytokine

staining (ICS), cells were fixed and permeabilised using the CytoFix/CytoPerm kit (BD Biosciences). For cell surface phenotyping and functional assays *in vitro*, the following antibodies were used: CD14-PE/Cy7 (M5E2), CD14-BV650 (M5E2), CD45-V500 (HI30), CD206-PE/CF594 (19.2), CD206-BUV395 (19.2), TNFα-PE (MAb11), TNFα-AF700 (MAb11), CCL4-APC-H7 (D21-1351), GM-CSF-PE/CF594 (BVD2-21C11) and IL-6-BV421 (MQ2-13A5) [BD Biosciences]; CD3-FITC (UCHT1), CD20-FITC (2H7), CD16-BV711 (3G8) and HLA-DR-BV785 (L243) [Biolegend]; CD56-FITC (MEM188) [eBioscience]; CD116-PE/Vio770 (REA211) [Miltenyi Biotec]; CCL3-FITC (93342) [R&D]; CD88-PE (S5/1) [ExBio]. For cell surface phenotyping related to *in vitro* and *in vivo* GM-CSF blocking experiments, the following antibodies were used: CD3-BV650 (SP34-2), CD5-BV711 (UCHT2), CD14-PE/Cy7 (M5E2), CD14-AF700 (M5E2), CD19-BV650 (SJ25C1), CD20-BV650 (2H7), CD45-V500 (HI30), CD45RA-FITC (5H9), CD123-BUV395 (7G3), CD169-PE (7-239), CD206-PE/CF594 (19.2), CD206-BUV395 (19.2) and streptavidin-BUV737 [BD Biosciences]; CD1c-BV421 (L161), CD3-FITC (UCHT1), CD16-APC/Cy7 (3G8), CD88-PerCP/Cy5.5 (S5/1), CD88-PE/Cy7 (S5/1), CD163-BV605 (GHI/61), FcεRIα-PerCP (AER-37) and HLA-DR-BV785 (L243) [Biolegend]; Mouse CD45-Biotin (30-F11) [eBioscience]; SynCAM/CADM1 (3E1) [MBL Life Science]; Chicken IgY-AF647 (polyclonal) [Jackson Immunoresearch]. Mononuclear cells isolated from humanised mouse tissues were quantified using CountBright Absolute Counting Beads (Invitrogen) by adding half the recommended amount. Data were analysed using FACSDiva (BD Biosciences) software.

### Unsupervised analysis of flow cytometric data by t-SNE and PhenoGraph

t-distributed stochastic neighbour embedding (t-SNE) and PhenogGraph analyses were performed as previously described.[2,25] FCS files compensated for spillover between channels were exported using FlowJo v10 (Tree Star Inc.). FCS files were then imported into the R environment via the read. FCS function in the flowCore package and intensity values of marker expression were extracted. The intensity values of marker expression were then logicle-transformed via the logicleTransform function in the flowCore package using parameters w = 0.1, t = 4,000, m = 4.5 and a = 0. Subsequently up to 20,000 cell events were randomly sampled from individual FCS files and combined. The dimensionality of the combined data was reduced to 2 using bh_tsne, an efficient implementation of t-SNE via Barnes-Hut approximations. Lastly the 2D t-SNE coordinates were inverse-logicle transformed and added to the original FCS files as additional channels. PhenoGraph algorithm was applied using a script in R obtained from Jinmiao Chen's laboratory (https://github.com/JinmiaoChenLab/Rphenograph) to automatically define landmark clusters.

### *In vitro* assays

PBMCs were cultured in RPMI (Gibco) supplemented with 10% FCS (R10) at 37°C, 5% $CO_2$. For cell surface phenotyping and functional assays, frozen PBMCs were thawed and seeded in either 48-well ($1.5\times10^6$ cells/ml) or 96-well plates ($2.5–3.75\times10^6$ cells/ml) and cultured for 24 h to 48 h. Functional assays were performed by priming cells with recombinant human GM-CSF (100 ng/ml; R&D), LPS (10pg/ml; Invivogen) or both for 24 h or 48 h and subsequently challenged with LPS (10 ng/ml) for 6 h in the presence of brefeldin A (10μg/ml; Sigma-Aldrich). For GM-CSF blocking experiments, fresh or thawed PBMCs were seeded in either 48-well ($1.5\times10^6$ cells/ml) or 96-well ($3.75\times10^6$ cells/ml) plates and treated with anti-GM-CSF neutralising antibody (10μg/ml; Miltenyi Biotec) or isotype antibody (Miltenyi Biotec) for 24 h or 48 h. Cells were then labelled for flow cytometric analysis.

### Serum analyses

Cytokine, except GM-CSF in human serum, concentrations from human and humanised mouse sera were measured using human cytokine bead-based assays (Luminex). Human serum GM-CSF was quantified using the high sensitivity GM-CSF ELISA kit (R&D Systems). Serum soluble CD14 (sCD14) from humanised mice was quantified using the human sCD14 ELISA kit (R&D Systems) or the human sCD14 flex set (BD Biosciences) respectively.

### Humanised mouse model

Non-obese diabetic (NOD) SCID gamma (NSG) humanised mice (17 females and 7 males, with no difference in reconstitution) were established from $CD34^+$ hepatic stellate cells (HSCs) of foetal liver tissues (single donor) as described previously.[2,26] The mice were bled 8–10 weeks post-transplantation to determine the human immune reconstitution and serum human albumin levels. 10 to 12-week-old mice (10–70% human immune cell reconstitution; serum hAlbumin 20–200 ng/ml) were infected with $10^7$IU of HBV (genotype D3, from HepG2.2.15 or HepAD38 cells) by intravenous injection (day 0). To deplete gut microbiota, penicillin G Sodium (1 mg/ml) and streptomycin sulfate (2 mg/ml) antibiotics were given 1 week before infection and subsequently twice a week in drinking water. For GM-CSF blocking *in vivo*, intravenous anti-GM-CSF neutralising antibody (1 mg/kg; Miltenyi Biotec) was administered 1 day prior to HBV inoculation (prophylactic group) and once a week thereafter and starting from week 6 for the therapeutic group. The control group received the same volume of PBS weekly starting from the day prior to HBV inoculation. Serum HBV DNA was purified using QIAamp MinElute Viral Spin kit (Qiagen) and measured by qPCR using primers designed previously and standards (Applied Biosystems). Serum alanine aminotransferase (ALT) was measured by the comparative medicine in house veterinary diagnostic laboratory, National University of Singapore, as previously described.[26] All experimental procedures were approved by the Institutional Animal Care and Use Committee (IACUC). All mice were bred and kept under specific pathogen-free with 12 h light/12 h dark cycle conditions in Biological Resource Centre, Agency for Science, Technology and Research, Singapore in accordance with the guidelines of the Agri-Food and Veterinary Authority and the National Advisory Committee for Laboratory Animal Research of Singapore. To avoid overcrowding, a maximum of 5 mice per cage was allowed. All mice were fed with irradiated TEKLAD GLOBAL 18% Protein Rodent Diet (2918) and water and monitored daily for health. Changes of mice cages were conducted on a weekly basis.

### Histological analyses of humanised mouse liver

All mice were sacrificed at 10 weeks post HBV infection. Liver tissues were processed as previously described.[26] Briefly, liver tissues were fixed in 10% formalin prior to paraffin block embedment. Rehydrated tissues sections were stained with H&E (Thermo Scientific), Fast-Green (Sigma) & Sirius Red (Sigma) according to manufacturer's protocol. Quantification of liver

fibrosis was measured by area of fibrotic lesions stained with Sirius Red over observed whole region of interest using the ImageJ software. All images were captured by the ZEISS Axio Scan.Z1 and processed using the Zen lite software.

### Real-time PCR

RNA was extracted from liver tissues using TRIzol Reagent (Invitrogen) followed by reverse transcription to cDNA via QuantiTect Reverse Transcription Kit (Qiagen) according to manufacturer's instructions. DNA template was added into SsoFast EvaGreen Supermix (BIO-RAD) with paired primers of interest prior to real-time PCR using BIO-RAD's CFX Connect Real-Time PCR Detection System. Primer sequences are available in Table S2. The relative abundance of mRNA expression of a control sample was arbitrarily designated as 1, and the values of the relative abundance of mRNA of other samples were calculated accordingly.

### Statistical analyses

Statistical analyses were performed using GraphPad Prism 6. The Mann-Whitney test (2-tailed) was used in all data analyses apart from where cells from the same donor were subjected to different treatment conditions or the same animals were followed longitudinally, in which cases the Wilcoxon signed-rank test (2-tailed) was used. Differences were defined as statistically significant when $p$ <0.05.

### Study approval

All clinical specimens were collected with written informed consent prior to inclusion in the study in accordance with the Declaration of Helsinki and local research ethics committee approval. Animal experimental procedures were in accordance with protocols approved by the International Animal Care and Use Committee (IACUC) at the Biological Resource Centre in A*STAR, Singapore.

## Results

### Liver fibrosis correlates with intrahepatic GM-CSF and CD206$^+$ macrophages in patients with viral- and non-viral-related liver disease

In our previous study,[2] we showed that in comparison to healthy livers, cirrhotic human livers were enriched with CD14$^+$HLA-DR$^{hi}$CD206$^+$ macrophages which spontaneously produced tumour necrosis factor-α (TNFα) and were more refractory to endotoxin-induced tolerance, a mechanism involving GM-CSF. While GM-CSF has been implicated as a central mediator of neurological and articular inflammation, its role in chronic liver inflammation has not been investigated. We first carried out confocal microscopy experiments on the non-tumour regions of liver tissue from a patient with hepatocellular carcinoma and confirmed that intrahepatic CD14$^+$ macrophages produced GM-CSF as observed by the intracytoplasmic detection of GM-CSF within macrophages (Fig. 1A). To better understand the interplay between TNFα-producing CD206$^+$ macrophages and GM-CSF within human livers, we next carried out multiplex immunofluorescence analyses on the non-tumour regions of liver tissue from patients with HCC (n = 47) secondary to viral or non-viral aetiologies (Table 1). Using the inForm software, individual cells in each image were delineated. For each cell, the mean cytoplasmic fluorescence intensities of each staining were measured and further analysed by histo-cytometry. CD14$^-$CK-18$^{+/-}$ cells were defined as non-macrophage cells and CD14$^+$ cells as macrophages with CD206$^+$ detected mostly on macrophages (Fig. 1B). TNFα and GM-CSF were quantified in total macrophages, subsets of CD206$^-$ and CD206$^+$ macrophages and in CD14$^-$CK-18$^{+/-}$ cells (Fig. 1C). Using the spatial coordinates of each cell, we observed that CD14$^+$CD206$^-$ macrophages were found lining blood vessels (perivascular area) while CD14$^+$CD206$^+$ macrophages were detected mostly in the liver stroma/parenchyma in highly fibrotic (fibrosis score = 6) livers (Fig. 1D-F and S1A). Co-localisation of GM-CSF with CD14 was also evaluated in immunofluorescence images as exemplified for images obtained for patient TMA-18 (Fig. S1B-C).

Apart from a non-significant trend toward an increased density of TNFα$^+$ macrophages in HCV+ patients, no quantitative difference was observed between patients based on HBV or HCV infection status (Fig. S1D), but we observed striking differences when dividing patients based on the degree of liver fibrosis by Ishak scoring[21,22] (Fig. 1G-J). We observed that highly fibrotic livers (Ishak 3-6, n = 33) had a greater density of CD206$^+$ (but not CD206$^-$) macrophages compared to mildly fibrotic livers (Ishak 0-2, n = 14) (Fig. 1G-H). We also confirmed that CD206$^+$ macrophages produced more TNFα and GM-CSF than their CD206$^-$ counterparts and that this production was increased in highly fibrotic livers (Fig. 1I-J, and Fig. S1D). Although the frequency of GM-CSF producing CD14$^-$CK-18$^{+/-}$ non-macrophages producing cells was higher than that of GM-CSF-producing CD14$^+$ macrophages (Fig. S1F), the numbers of CD206$^+$ macrophages strongly correlated with the numbers of GM-CSF-producing macrophages but not with that of GM-CSF-producing CD14$^-$CK-18$^{+/-}$ cells (Fig. 1K). Finally, the numbers of intrahepatic GM-CSF$^+$ and TNFα$^+$ macrophages were positively correlated (Fig. 1L). Collectively, the accumulation of TNFα- and GM-CSF- producing intrahepatic CD206$^+$ macrophages is positively correlated with the degree of liver fibrosis in human livers independent of aetiology.

### Elevated serum GM-CSF concentrations are associated with advanced liver fibrosis and systemic inflammation in patients with viral-related liver disease

Having identified a link between intrahepatic GM-CSF expression by CD206$^+$ macrophages and liver fibrosis, we sought to validate this observation in cohorts of non-HCC liver disease patients. To this end, we measured the serum concentration of GM-CSF, along with TNFα and IL-1β, in chronic HCV-infected (CHC; divided into low [<5×10$^5$IU/ml, n = 12] and high [>1 ×10$^6$IU/ml, n = 17] plasma HCV RNA [Table 2]) patients before the initiation of DAA therapy and compared them to healthy human donors (n = 7). Serum GM-CSF was higher in CHC patients with high viremia compared to healthy controls and to patients with low viremia (Fig. 2A, left panel), while only a non-significant trend to increased serum GM-CSF was observed when patients were split based on their serum ALT concentration (Fig. S2A). The concentration of serum TNFα was also elevated in high viremia patients but did not reach statistical significance (Fig. 2A, right panel). The serum concentration of GM-CSF in all CHC patients was significantly positively correlated with that of TNFα and IL-1β (Fig. 2B), suggesting that the elevated serum GM-CSF concentration during chronic HCV infection is associated with an inflammatory response, as previously described.[27,28] Since we observed no difference in serum GM-CSF concentrations before and after therapy (Fig. S2B), all patients in this cohort, both before and after DAA therapy, were

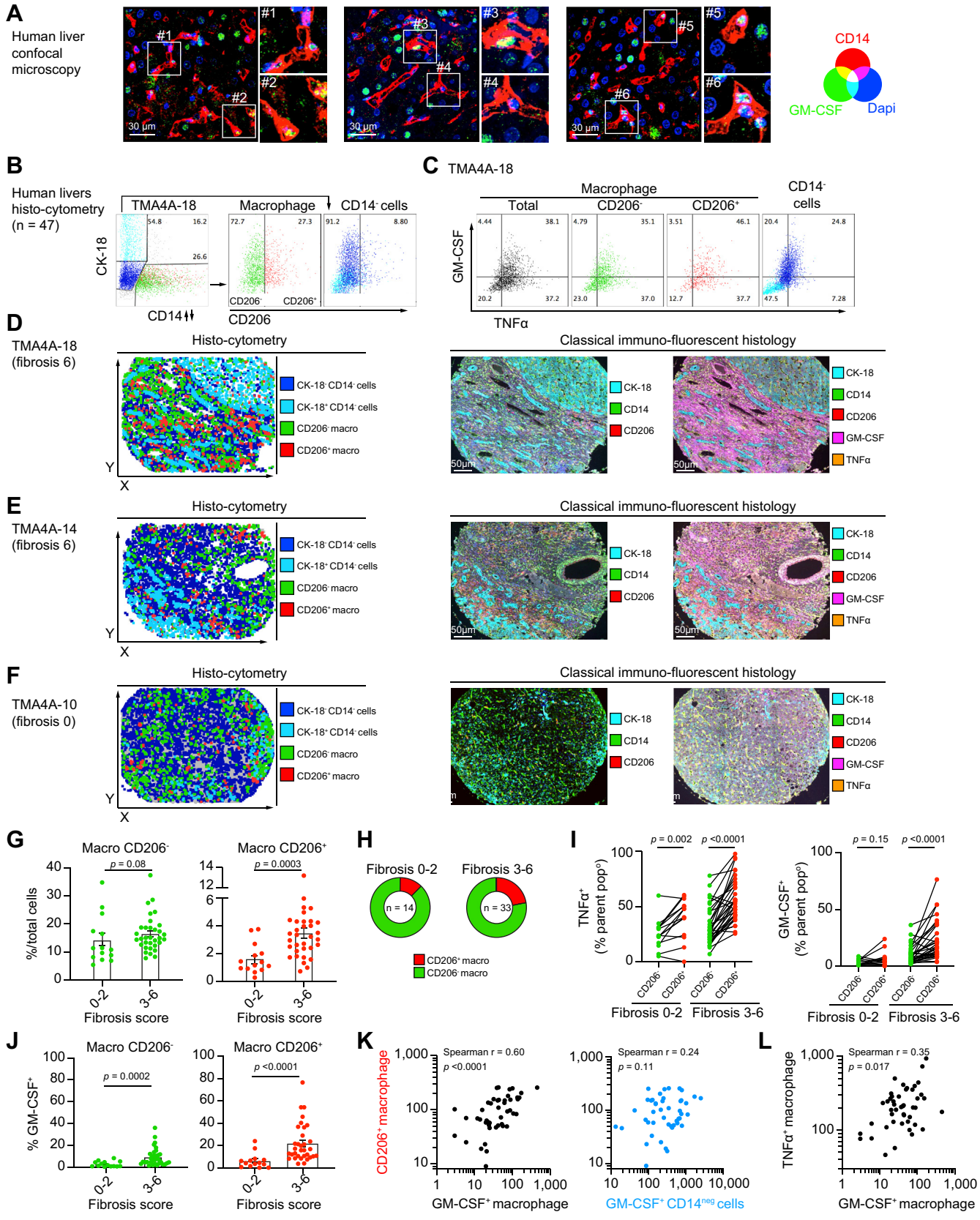


**Fig. 1. Liver fibrosis correlates with intrahepatic GM-CSF and CD206$^+$ macrophages in patients with viral- and non-viral-related liver disease.** (A) CD14 (red), GM-CSF (green) and DAPI (blue) 3-color confocal microscopy images of a human liver cross-section are shown. Two insets displaying GM-CSF-containing CD14+ macrophages are displayed for each large field images. (B-L) Histo-cytometry analysis of the cytoplasmic mean fluorescence of each single cell delineated in non-tumour regions of liver specimens from patients diagnosed with HCC (n = 47). (B) Gating strategy (histo-cytometry) for patient TMAA4A-18 defining

then segregated based on liver fibrosis as determined by transient elastography (Fibroscan). Compared to patients with a fibrosis score of zero, serum GM-CSF and TNFα concentrations were significantly increased in patients with high fibrosis score (3+4) but contrary to TNFα, GM-CSF increase was not significant in patients with an intermediate fibrosis score (1+2) (Fig. 2C).

We next quantified serum GM-CSF concentrations in a cohort of patients with NASH (n = 18), for which fibrosis was scored (Table 3). The lower number of included patients compared to the previous cohort did not allow us to observe significant differences between patients with NASH and healthy controls, although a trend to increased serum GM-CSF concentration was observed in patients (Fig. S2C). Interestingly, we observed that as for patients with HCV and a higher fibrosis score, the 3 patients with NASH and the highest fibrosis score (= 4) had significantly increased serum GM-CSF concentrations compared to healthy controls and to patients with NASH and low fibrosis score (= 1; Fig. 2D). Therefore, circulating GM-CSF levels may correlate with the degree of liver fibrosis and systemic inflammation in chronic liver disease of different aetiologies including HCV infection and NASH.

### Differentiation of TNFα-producing CD206$^+$ monocyte-derived macrophages is driven by LPS in a GM-CSF-dependent manner

To investigate the mechanism leading to GM-CSF overproduction and CD206$^+$ macrophage accumulation and since chronic liver disease is associated with increased gut microbial translocation and liver inflammation,[29–31] we utilised a humanised (HIL) mouse model of viral-induced liver disease and measured the concentration of serum GM-CSF in mock- (n = 11) and HBV-infected (n = 13) animals before and after administration of oral antibiotics at 6–16 weeks post-infection (wpi) (Fig. 3A-B). GM-CSF was significantly higher in HBV-infected than mock-infected animals and this increase was abrogated following antibiotic treatment (Fig. 3A). We also observed that serum GM-CSF concentrations in HIL mice were significantly positively correlated with both serum soluble CD14 (sCD14, a marker of bacterial translocation and myeloid cell activation[29]) and the frequency of intrahepatic CD206$^+$ macrophages (Fig. 3B). We next studied the interplay between bacterial products (LPS), GM-CSF and human TNFα-producing CD206$^+$ monocyte-derived macrophage-like cells (moMΦs) *in vitro*. First, we confirmed that human monocytes can produce GM-CSF in response to LPS (Fig. S3A).[32] Next, healthy human PBMCs were primed with or without recombinant human GM-CSF (rhGM-CSF) and subsequently challenged with LPS (10ng/ml). Unsupervised analysis of flow cytometric data using t-SNE and PhenoGraph identified 4 clusters of cells (#2, #4, #5 and #9) among HLA-DR$^+$CD88$^+$ myeloid cells which upregulated CD206 expression upon GM-CSF and/or LPS treatment (Fig. 3C-D and Fig. S3B-C). Except for cluster #2, the remaining clusters also upregulated the cytokines TNFα, IL-6 and GM-CSF and the chemokines CCL3 and CCL4 (Fig. 3C-D and Fig. S3C), which is further illustrated by manual gating (Fig. 3E and Fig. S3D). Importantly, the majority of cells that produced these cytokines and chemokines were CD206$^+$, but not CD206$^-$, cells. Peripheral blood monocytes from healthy human donors (n = 7) primed with rhGM-CSF for 24 h showed a significantly higher frequency of CD206$^+$ cells compared to untreated controls (Fig. 3F), consistent with previous reports showing that GM-CSF can upregulate the expression of CD206 on monocytes.[33–35] Priming of monocytes with LPS alone was sufficient to induce a significantly higher frequency of CD206$^+$/CD14$^{hi}$ cells compared to untreated controls, although the extent of CD206 induction was lower than that achieved with rhGM-CSF (Fig. 3F-G). Peripheral blood monocytes primed with rhGM-CSF and subsequently challenged with LPS showed a significantly higher frequency of TNFα$^+$CD14$^{hi}$CD206$^+$ and IL-6$^+$CD14$^{hi}$CD206$^+$ cells compared to monocytes cultured without rhGM-CSF (Fig. 3H and Fig. S3E, left panels). Interestingly, this proinflammatory effect of GM-CSF was specific to CD14$^{hi}$CD206$^+$ cells and was not seen in CD14$^{hi}$CD206$^-$ cells (Fig. 3H and Fig. S3E, right panels). Therefore, GM-CSF and LPS can promote the differentiation of TNFα-producing CD206$^+$ moMΦ. To determine if CD206$^+$ moMΦ differentiation from CD14$^+$ monocytes when exposed to LPS was dependent on GM-CSF production, we treated LPS-activated healthy human PBMCs (n = 7) with either anti-GM-CSF neutralising antibody or isotype control for 24 h. In the presence of isotype antibody, we confirmed that LPS activation resulted in a significantly higher frequency of CD14$^+$CD206$^+$ cells among CD14$^{hi}$CD88$^{hi}$ cells compared to unstimulated controls (Fig. 3I). Treatment with anti-GM-CSF antibody abrogated this increase in frequency of CD14$^+$CD206$^+$ cells following LPS activation (Fig. 3I-J). These results demonstrated *in vitro* that bacterial products (LPS) can induce GM-CSF production by monocytes, which in turn can induce their conversion into TNFα-producing CD206$^+$ moMΦ.

### GM-CSF neutralisation inhibits intrahepatic CD206$^+$ macrophage accumulation and fibrosis in viral-induced liver disease

Our next aim was to evaluate *in vivo* the role of GM-CSF in liver fibrosis and CD206$^+$ macrophage accumulation,[2] using the same HBV-induced liver inflammation model as in Fig. 3A-B (HBV-infected NSG humanised mice). To this end, HBV-infected animals were treated with a neutralising anti-GM-CSF antibody either prophylactically (treatment started the day of the HBV infection, D0), or therapeutically (treated 6 weeks

CD14$^-$CK-18$^+$ hepatocytes (cyan), CD14$^-$CK-18$^-$ cells (blue), CD14$^+$ macrophages, CD206$^-$ (green) and CD206$^+$ (red) macrophage subsets. (C) Dot plots of TNFα and GM-CSF expression by total macrophages (grey), CD206$^-$ (green) and CD206$^+$ (red) macrophage subsets, and CD14$^-$CK-18$^{+/-}$ cells (blue and cyan). (D-F) Using the spatial coordinates of each cell, the localisation in liver cross-sections of the 4 cell subsets defined in (B) are displayed for (D) patient TMAA4A-18, for (E) patient TMAA4A-14 (both with a fibrosis score of 6) and (F) patient TMAA4A-10 (fibrosis score of 0). Corresponding immunofluorescence images showing expression of Cytokeratin-18 (CK-18)/CD14/CD206 (middle panels) and of CD14/CD206/GM-CSF/TNFα (right panels) for these 3 patients are displayed. (G-J) Data from patients based on a low (Ishak 0-2) or high (Ishak 3-6) fibrosis score are displayed as mean. (G-H) Proportion of CD206$^-$ and CD206$^+$ macrophages among (G) total cells or (H) among total macrophages in patients with low (Ishak 0-2, n = 14) or high (Ishak 3-6, n = 33) fibrosis scores. (I) Comparison of the proportion of CD206$^-$ and CD206$^+$ macrophages positive for TNFα (left panel) or GM-CSF (right panel). (J) Proportion of GM-CSF-producing CD206$^-$ (left panel) and CD206$^+$ (right panel) macrophages in patients with low or high fibrosis scores. (K) Correlative analysis of total counts of CD206$^+$ macrophages and GM-CSF$^+$ macrophages (left panel) or GM-CSF$^+$ CD14$^-$CK$^{+/-}$ cells (right panel). (L) Correlative analysis of total counts of TNFα$^+$ macrophages and GM-CSF$^+$ macrophages. *p* values calculated by Mann-Whitney test for (G,J), by Wilcoxon signed-rank test for (I) and by Spearman's correlation for (K-L). HCC, hepatocellular carcinoma; TMA, tissue microarray.

**Table 2. Clinical data of chronic HCV patients used in this study.**

| Patient code | [a]Age | HCV geno-type | HCV RNA (IU/ml) | Platelets ($\times 10^3$/ blood µl) | AST (U/L) | ALT (U/L) | Transient elastography - Fibroscan (LSM, kPa) | Corresponding fibrosis stage | DAA therapy | DAA therapy, duration (weeks) | DAA therapy: stable or worsened (S/W); improved (I) |
|---|---|---|---|---|---|---|---|---|---|---|---|
| A1 | 75 | 2 | 1,889,973 | 120 | 68 | 66 | 21.3 | F4 | No | 20 | Before therapy |
| A2 | 71 | 2 | 1,752,096 | 178 | 77 | 33 | 45 | F4 | No | 16 | Before therapy |
| A3 | 41 | 3 | 30,542 | 111 | 28 | 33 | 11.9 | F3 | No | 12 | Before therapy |
| A4 | 54 | 1a | 1,339,421 | 68 | 48 | 44 | 21 | F4 | No | 12 | Before therapy |
| A5 | 75 | 1b | 1,282,949 | 57 | 101 | 101 | 12.3 | F4 | No | 12 | Before therapy |
| A6 | 33 | 2 | 176,174 | 325 | 35 | 35 | 7.3 | F2 | No | 12 | Before therapy |
| A7 | 75 | 2 | 2,518,848 | 68 | 52 | 51 | 10.3 | F3 | No | 20 | Before therapy |
| A8 | 59 | 1b | 418,946 | 264 | 63 | 114 | 13 | F4 | No | 12 | Before therapy |
| A9 | 52 | 4 | 2,261,525 | 211 | 26 | 26 | 8.5 | F2 | No | 12 | Before therapy |
| A10 | 79 | 1b | 156,715 | 69 | 52 | 24 | 13.1 | F4 | No | 12 | Before therapy |
| A11 | 61 | 1b | 85,907 | 84 | 47 | 49 | 12.9 | F4 | No | 12 | Before therapy |
| A12 | 28 | 4 | 40,581 | 96 | 110 | 113 | 26.6 | F4 | No | 12 | Before therapy |
| A13 | 72 | 1b | 595,543 | 131 | 48 | 46 | 12.2 | F4 | No | 12 | Before therapy |
| A14 | 53 | 4 | 955,001 | 151 | 39 | 47 | 10.7 | F3 | No | 12 | Before therapy |
| A15 | 70 | 1b | 120,362 | 221 | 38 | 53 | 10.5 | F3 | No | 12 | Before therapy |
| A16 | 74 | 1b | 1,891,709 | 268 | 60 | 85 | 12 | F4 | No | 12 | Before therapy |
| A17 | 74 | 1b | 846,395 | 174 | 45 | 58 | 7.6 | F2 | No | 12 | Before therapy |
| A18 | 33 | 1b | 5,357,173 | 212 | 56 | 79 | 7 | F2 | No | 12 | Before therapy |
| A19 | 47 | 1b | 618,236 | 198 | 22 | 25 | 3.5 | F0 | No | 12 | Before therapy |
| A20 | 32 | 4 | 104,347 | 262 | 44 | 62 | 3.3 | F0 | No | 12 | Before therapy |
| B1 | 66 | 2 | 913,475 | 153 | 237 | 210 | 14.9 | F4 | No | 12 | Before therapy |
| B2 | 76 | 2 | 723,350 | 124 | 123 | 119 | 34.3 | F4 | No | 20 | Before therapy |
| B3 | 76 | 1b | 1,605,414 | 165 | 61 | 64 | 13.7 | F4 | No | 12 | Before therapy |
| B4 | 68 | 2 | 37,578 | 198 | 46 | 44 | 16.5 | F4 | No | 24 | Before therapy |
| B5 | 52 | 1b | 113,069 | 471 | 73 | 59 | 19.6 | F4 | No | 12 | Before therapy |
| B6 | 59 | 4 | 2,379,329 | 131 | 78 | 118 | 34.3 | F4 | No | 12 | Before therapy |
| B7 | 52 | 1b | 787,577 | 170 | 50 | 94 | 13.8 | F4 | No | 12 | Before therapy |
| B8 | 45 | 3 | 1,950,045 | 172 | 181 | 321 | 7.3 | F2 | No | 12 | Before therapy |
| B9 | 54 | 3 | 301,056 | 194 | 47 | 49 | 9.9 | F3 | No | 12 | Before therapy |
| B10 | 75 | 2 | 1,267,225 | 234 | 234 | 429 | 8.8 | F2 | No | 12 | Before therapy |
| B11 | 61 | 2 | 345,743 | 180 | 118 | 148 | 10.3 | F3 | No | 12 | Before therapy |
| B12 | 48 | 1a | 182,706 | 213 | 111 | 202 | 10.8 | F3 | No | 12 | Before therapy |
| B13 | 60 | 3 | 1,870,235 | 106 | 92 | 74 | 10.4 | F3 | No | 12 | Before therapy |
| B14 | 50 | 1b | 1,148,525 | 269 | 107 | 134 | 12 | F4 | No | 12 | Before therapy |
| B15 | 51 | 3 | 522,615 | 251 | 109 | 151 | 11.3 | F3 | No | 12 | Before therapy |
| B16 | 60 | 4 | 1,172,663 | 206 | 40 | 57 | 10.7 | F3 | No | 12 | Before therapy |
| B17 | 52 | 4 | 3,969,720 | 171 | 39 | 58 | 10.5 | F3 | No | 24 | Before therapy |
| B18 | 72 | 1b | 296,760 | 224 | 37 | 45 | 10.7 | F3 | No | 12 | Before therapy |
| B19 | 56 | 1a | 530,845 | 165 | 58 | 76 | 10.8 | F3 | No | 12 | Before therapy |
| B20 | 72 | 1b | 1,909,834 | 178 | 68 | 60 | 12.1 | F4 | No | 12 | Before therapy |
| SVRA1 | 76 | 2 | 0 | 111 | 24 | 17 | 22.8 | F4 | SOF + RBV | 20 | S/W |
| SVRA2 | 72 | 2 | 0 | 100 | 85 | 31 | 75 | F4 | SOF + RBV | 16 | S/W |
| SVRA3 | 42 | 3 | 0 | 120 | 20 | 21 | 11.9 | F4 | SOF + RBV | 12 | S/W |
| SVRA4 | 54 | 1a | 0 | 76 | 21 | 17 | 21.3 | F4 | SOF/LDV | 12 | S/W |
| SVRA5 | 75 | 1b | 973,666 | 58 | 72 | 78 | 21.8 | F4 | SOF/LDV | 12 | S/W |
| SVRA6 | 33 | 2 | 0 | 255 | 15 | 11 | 14.3 | F4 | SOF + DCV | 12 | S/W |
| SVRA7 | 75 | 2 | 0 | 68 | 48 | 42 | 12.8 | F4 | SOF + RBV | 20 | S/W |
| SVRA8 | 59 | 1b | 0 | 220 | 17 | 22 | 14.5 | F4 | 3D | 12 | S/W |
| SVRA9 | 53 | 4 | 0 | 195 | 15 | 13 | 8.8 | F2 | 2D + RBV | 12 | S/W |
| SVRA10 | 79 | 1b | 0 | 75 | 43 | 21 | 72 | F4 | SOF/LDV | 12 | S/W |
| SVRA11 | 61 | 1b | 0 | 76 | 15 | 11 | 21.5 | F4 | 3D | 12 | S/W |
| SVRA12 | 28 | 4 | 0 | 106 | 31 | 38 | 30.7 | F4 | SOF + SMV | 12 | S/W |
| SVRA13 | 72 | 1b | 0 | 130 | 18 | 14 | 13.2 | F3 | SOF + SMV | 12 | S/W |
| SVRA14 | 54 | 4 | 0 | 164 | 18 | 20 | 12 | F4 | 2D + RBV | 12 | S/W |
| SVRA15 | 71 | 1b | 0 | 227 | 20 | 16 | 10.1 | F3 | 3D | 12 | S/W |
| SVRA16 | 75 | 1b | 0 | 271 | 21 | 7 | 11.8 | F3 | SOF/LDV | 12 | S/W |
| SVRA17 | 74 | 1b | 0 | 140 | 31 | 28 | 7.1 | F2 | SOF/LDV | 12 | S/W |
| SVRA18 | 33 | 1b | 0 | 207 | 27 | 22 | 6.7 | F2 | 3D | 12 | S/W |
| SVRA19 | 48 | 1b | 0 | 207 | 20 | 14 | 3.4 | F0 | EBR/GRZ | 12 | S/W |
| SVRA20 | 33 | 4 | 0 | 279 | 23 | 20 | 3.4 | F0 | 2D + RBV | 12 | S/W |
| SVRB1 | 67 | 2 | 0 | 132 | 49 | 44 | 8.9 | F2 | SOF + DCV | 12 | I |
| SVRB2 | 77 | 2 | 0 | 112 | 41 | 37 | 19.1 | F4 | SOF + RBV | 20 | I |
| SVRB3 | 77 | 1b | 0 | 172 | 20 | 13 | 8.4 | F2 | 3D | 12 | I |
| SVRB4 | 69 | 2 | 0 | 173 | 32 | 23 | 8.3 | F2 | SOF + RBV | 24 | I |
| SVRB5 | 53 | 1b | 0 | 412 | 29 | 19 | 10.4 | F3 | 3D | 12 | I |
| SVRB6 | 60 | 4 | 0 | 209 | 32 | 40 | 18 | F4 | 2D + RBV | 12 | I |

(*continued on next page*)

**Table 2** (*continued*)

| Patient code | [a]Age | HCV geno-type | HCV RNA (IU/ml) | Platelets (×10$^3$/ blood µl) | AST (U/L) | ALT (U/L) | Transient elastography - Fibroscan (LSM, kPa) | Corresponding fibrosis stage | DAA therapy | DAA therapy, duration (weeks) | DAA therapy: stable or worsened (S/W); improved (I) |
|---|---|---|---|---|---|---|---|---|---|---|---|
| SVRB7 | 53 | 1b | 0 | 139 | 17 | 19 | 6 | F1 | 3D | 12 | I |
| SVRB8 | 46 | 3 | 0 | 214 | 31 | 41 | 3.3 | F0 | SOF + DCV | 12 | I |
| SVRB9 | 55 | 3 | 0 | 260 | 18 | 16 | 4.9 | F0 | SOF + DCV | 12 | I |
| SVRB10 | 76 | 2 | 0 | 213 | 21 | 17 | 5.7 | F0 | SOF + RBV | 12 | I |
| SVRB11 | 61 | 2 | 0 | 169 | 16 | 13 | 5.3 | F0 | SOF + RBV | 12 | I |
| SVRB12 | 49 | 1a | 0 | 243 | 26 | 26 | 6.9 | F1 | SOF/LDV + RBV | 12 | I |
| SVRB13 | 60 | 3 | 0 | 150 | 25 | 15 | 6.9 | F1 | SOF + DCV | 12 | I |
| SVRB14 | 52 | 1b | 0 | 296 | 26 | 29 | 5.4 | F1 | 3D | 12 | I |
| SVRB15 | 52 | 3 | 0 | 302 | 23 | 10 | 6 | F1 | SOF + DCV | 12 | I |
| SVRB16 | 61 | 4 | 0 | 224 | 16 | 13 | 6.6 | F1 | 2D + RBV | 12 | I |
| SVRB17 | 53 | 4 | 0 | 178 | 27 | 27 | 6.5 | F1 | 2D + RBV | 24 | I |
| SVRB18 | 72 | 1b | 0 | 242 | 17 | 10 | 8.7 | F2 | 3D | 12 | I |
| SVRB19 | 57 | 1a | 0 | 226 | 18 | 15 | 6.8 | F1 | 3D + RBV | 12 | I |
| SVRB20 | 73 | 1b | 0 | 184 | 28 | 21 | 7.8 | F2 | 3D | 12 | I |

[a] Age at sampling; DAA, direct-acting antivirals; SVR, sustained virological response; TMA, tissue microarray.

post-infection, wpi) and compared to control mice that had received an injection of saline solution (PBS) at D0 (Fig. 4A and Fig. S4A). In untreated HBV-infected mice (control group), we observed a progressive increase in serum sCD14 concentrations as early as 2 wpi which was abolished when anti-GM-CSF treatment was started at 0 wpi (prophylactic group), while it was only moderately reduced at 10 wpi when anti-GM-CSF treatment was started at 6 wpi (therapeutic group) (Fig. 4B). We also quantified serum concentrations of human ALT to evaluate liver damage, which indicated that intrahepatic inflammatory events had already commenced when animals from the therapeutic group started their anti-GM-CSF treatment (Fig. 4C). Interestingly, the significant increase of human ALT at 6 wpi was observed only in animals that were untreated (control and therapeutic groups), while the modest increase when comparing 0 wpi and 6 wpi was not significant in animals from the prophylactic group, suggesting that anti-GM-CSF limited liver damage already at 6 wpi. Importantly, administration of anti-GM-CSF neutralising antibodies significantly reduced the intrahepatic frequency and absolute number of CD206$^+$ macrophages compared to untreated controls (Fig. 4D and Fig. S4B). Serum sCD14 concentrations positively correlated with intrahepatic CD206$^+$ macrophage frequency suggesting that bacterial products may influence the accumulation of these cells (Fig. S4C). We next evaluated the impact of anti-GM-CSF treatment on liver fibrosis using Sirius Red staining (Fig. 4E-F). All mice in both prophylactic and therapeutic groups showed a significantly lower degree of liver fibrosis compared to mice in the control group (Fig. 4E-F). This observation was confirmed by a reduction in the hepatic expression of human pro-fibrotic genes in anti-GM-CSF treated mice (significant reduction only when comparing non-treated mice to mice from the therapeutic group, Fig. 4G and Fig. S4D). Finally, similar to our observation in human fibrotic livers (Fig. 1F-G), we also observed that the density of intrahepatic CD206$^+$ macrophages trended to correlate with liver fibrosis although not reaching statistical significance (Fig. 4H). This *in vivo* study demonstrates that GM-CSF contributes both to liver fibrosis and to CD206$^+$ macrophage accumulation during inflammatory liver disease.

## Discussion

Chronic liver disease is characterised by persistent inflammation leading to end-stage complications. Previously, we showed that intrahepatic TNFα-producing CD14$^+$HLA-DR$^{hi}$CD206$^+$ macrophages were expanded during viral-related liver disease possibly mediated by bacterial products such as LPS which are present in the gut flora.[2] In this study, we demonstrated that GM-CSF, like LPS, can promote CD206$^+$ monocyte-derived macrophage differentiation from monocytes. Both intrahepatic and circulating levels of GM-CSF positively correlated with liver fibrosis severity in patients with inflammatory liver disease independent of aetiology. Importantly, antibody-mediated neutralisation of GM-CSF reduced intrahepatic CD206$^+$ macrophage accumulation and liver fibrosis in a model of viral-induced liver disease, revealing for the first time a role of GM-CSF in liver fibrosis.

CD206 expression has traditionally been used to identify alternatively-activated (M2) macrophages, whose functions include, among others, immune regulation and tissue remodelling.[36,37] In our previous study[2] and here, we demonstrated that intrahepatic CD206$^+$ macrophages are potent TNFα and GM-CSF producers, proinflammatory functions conventionally associated with classically-polarised (M1) macrophages. Furthermore, we showed here that intrahepatic CD206$^+$ macrophages could be involved in liver fibrosis since they were proportionately enriched in patients with a higher degree of liver fibrosis and GM-CSF blockade reduced both their accumulation and liver fibrosis in HBV-infected humanised mice. Therefore, we provide further evidence that the M1/M2 paradigm, which was established by polarising monocytes *in vitro*, might be inadequate when describing tissue macrophage function *in vivo* due to the complexity of signals at play. A multidimensional approach to macrophage activation[38] may be more appropriate when analysing *in vivo* macrophage function. We postulate that CD206$^+$ macrophages may contribute to liver fibrosis in part via TNFα production. HSCs transdifferentiate into pro-fibrotic collagen-producing myofibroblasts upon activation,[39] and hepatic macrophages have been shown to promote HSC survival via TNF and IL-1 secretion both *in vitro* and *in vivo*, perpetuating liver fibrosis.[40] Furthermore, TNFα can upregulate pro-fibrotic TIMP-1

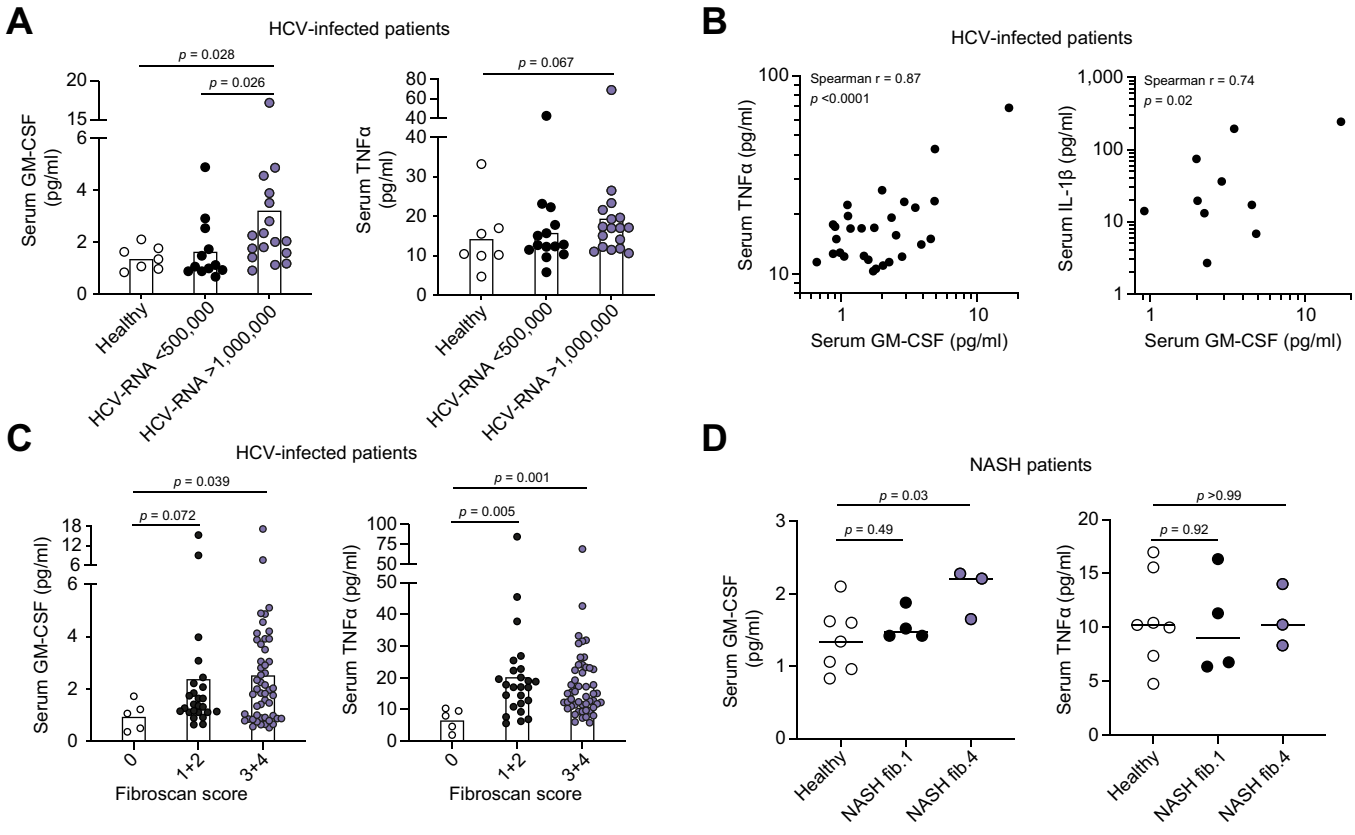


**Fig. 2. Elevated serum GM-CSF concentrations are associated with advanced liver fibrosis and systemic inflammation in patients with viral-related liver disease.** Serum GM-CSF (left panel) and TNFα (right panel) concentrations were measured by Luminex in (A) healthy human donors (n = 7) or CHC patients before DAA therapy with low (<$5\times10^5$IU/ml, n = 12) or high (>$1\times10^6$IU/ml, n = 17) viremia. Values are shown as mean concentration (pg/ml). (B) Correlative analyses of serum GM-CSF, TNFα and IL-1β concentrations from all CHC patients (high and low viremia) by Spearman's rank correlation coefficient. (C) Serum GM-CSF (left panel) and TNFα (right panel) concentrations were measured in all CHC patients (before and after DAA therapy) with a Fibroscan score of 0 (n = 5), 1-2 (n = 25) and 3-4 (n = 46 for GM-CSF, 4 out of range, and n = 50 for TNFα). (D) Serum GM-CSF (left panel) and TNFα (right panel) concentrations were measured in healthy controls (n = 7) and patients with NASH and a fibrosis score of 1 (n = 4) or of 4 (n = 3). *p* values calculated by Mann-Whitney test or Spearman's correlation. CHC, chronic hepatitis C; DAA, direct-acting antiviral; NASH, non-alcoholic steatohepatitis.

expression in HSCs[41] and downregulate the TGFβ pseudo-receptor Bambi, thus sensitising HSCs to the stimulatory effects of TGFβ.[42] Finally, TNF receptor knockout mice were found to have reduced HSC activation and TIMP-1 expression compared to wild-type mice in a methionine- and choline-deficient model of liver fibrosis.[43] Altogether, TNFα secretion by macrophages,

**Table 3. Clinical data of patients with NASH used in this study.**

| Subject number | Disease | Number of portal tracts | Steatosis grade (0-3) | Lobular inflammation (0-3) | Ballooning (0-2) | Fibrosis (0-4) |
|---|---|---|---|---|---|---|
| FLC_003 | NASH | 17 | 3 | 2 | 2 | 4 |
| FLC_008 | NASH | 10 | 1 | 2 | 2 | 4 |
| FLC_010 | NASH | 16 | 1 | 2 | 2 | 4 |
| FLC_018 | NASH | 14 | 1 | 2 | 2 | 2 |
| FLC_019 | NASH | 11 | 2 | 2 | 2 | 3 |
| FLC_024 | NASH | ≥11 | 1 | 3 | 2 | 3 |
| FLC_025 | NASH | ≥11 | 1 | 3 | 2 | 3 |
| FLC_026 | NASH | 9 | 2 | 2 | 2 | 2 |
| FLC_027 | NASH | 9 | 1 | 2 | 1 | 4 |
| FLC_028 | NASH | 10 | 2 | 2 | 1 | 3 |
| FLC_031 | NASH | ≥11 | 1 | 3 | 2 | 2 |
| FLC_032 | NASH | ≥11 | 1 | 3 | 2 | 3 |
| FLV_018 | NASH | 2 | 1 | 0 | 0 | 2 |
| FLV_027 | NASH | 2 | 1 | 0 | 0 | 1a |
| FLV_028 | NASH | 1 | 1 | 0 | 0 | 1a |
| FLV_032 | NASH | 2 | 1 | 0 | 0 | 2 |
| FLV_033 | NASH | 1 | 1 | 0 | 0 | 1a |
| FLV_041 | NASH | 2 | 1 | 0 | 0 | 1c |

NASH, non-alcoholic steatohepatitis.

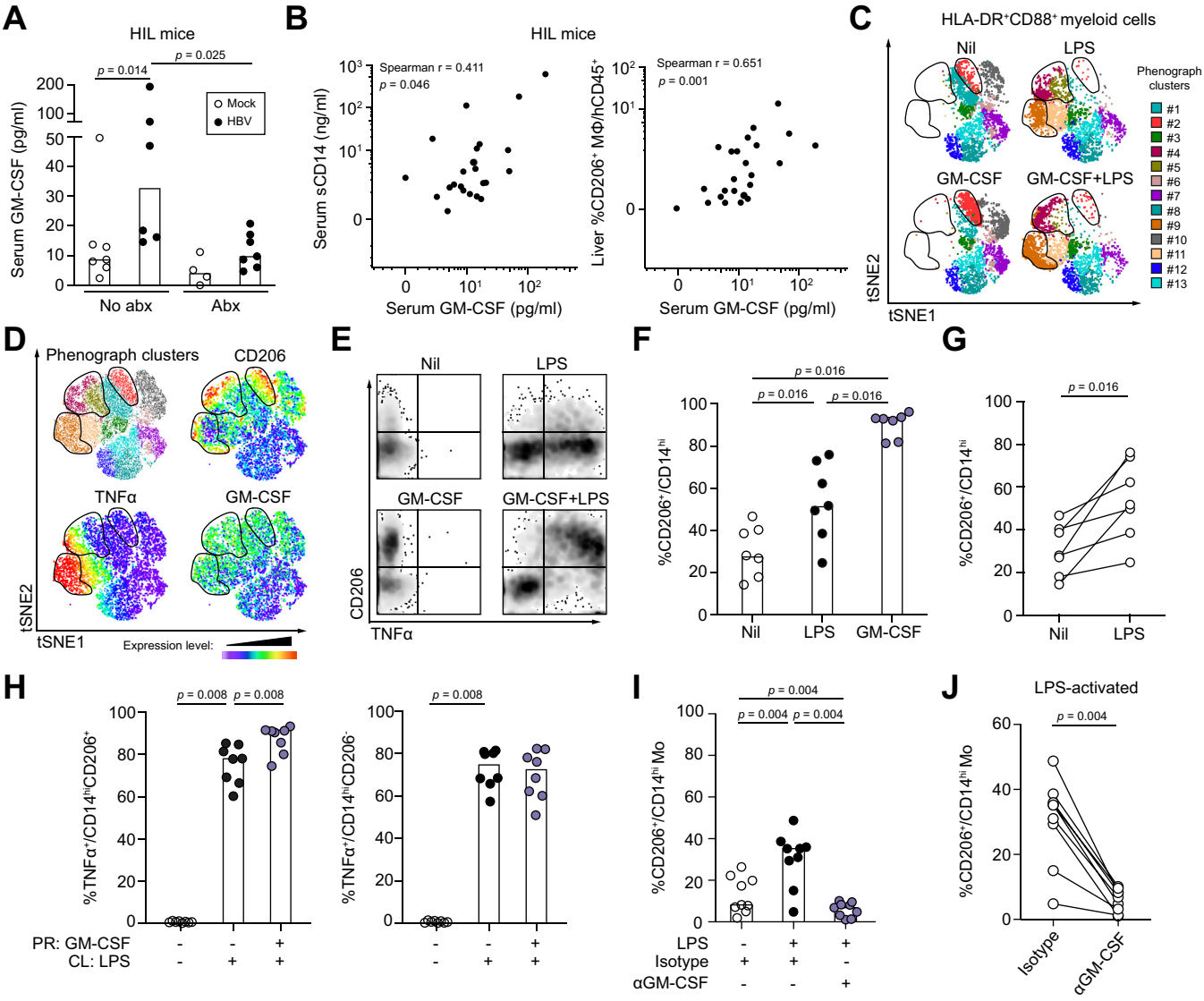


**Fig. 3. Differentiation of TNFα-producing CD206$^+$ monocyte-derived macrophages is driven by LPS in a GM-CSF-dependent manner.** (A) Serum GM-CSF concentrations in mock- (no abx n = 7; abx n = 4) and HBV-infected (no abx n = 6; abx n = 7) HIL mice with or without treatment with oral penicillin/streptomycin (1 mg/ml; 2 mg/ml) at 6-16 wpi. Values are shown as median concentration (pg/ml). (B) Correlative analyses of serum GM-CSF and sCD14 concentrations and intrahepatic CD14$^+$HLA-DR$^{hi}$CD206$^+$ cell frequency in mock- (n = 11) and HBV-infected (n = 13) HIL mice by Spearman's rank correlation coefficient. (C-J) Human PBMCs were primed *in vitro* in the presence or absence of GM-CSF (100 ng/ml) for 24 h and subsequently challenged with or without LPS (10 ng/ml) for 6 h. (C-D) Unsupervised analysis of single live CD45$^+$HLA-DR$^+$CD88$^+$ myeloid cells from flow cytometric data of healthy human peripheral blood (n = 1) by t-SNE and PhenoGraph clustering. Clusters (#1-13) were overlaid onto t-SNE dot plots and 3 CD206$^{hi}$ regions (clusters #2, #4, #5 and #9) were demarcated. (D) Concatenated t-SNE dot plot with clusters overlaid (upper left) and heatmaps showing the expression of CD206, TNFα and GM-CSF in the concatenated t-SNE plot (other panels). (E) Density plots of CD45$^+$HLA-DR$^+$CD88$^+$ cells from healthy human peripheral blood following 24 h priming with or without GM-CSF and subsequent challenge with LPS. The expression of TNFα and CD206 are shown. (F) Frequency of CD14$^{hi}$CD206$^+$ cells in healthy human PBMCs (n = 7) following 24 h priming with GM-CSF or LPS (10 pg/ml). Data are shown as median. (G) Frequency of CD14$^{hi}$CD206$^+$ cells in matched donors (n = 7) from the same dataset as (F) primed with or without LPS. (H) Frequency of TNFα$^+$ cells among CD14$^{hi}$CD206$^+$ (left panel) or CD14$^{hi}$CD206$^-$ (right panel) cells from healthy human PBMCs (n = 8) primed (PR) with or without GM-CSF for 24 h and subsequently challenged (CL) with LPS (10 ng/ml) for 6 h. (I) Frequency of CD14$^{hi}$CD206$^+$ cells in healthy human PBMCs (n = 9) following 24 h priming *in vitro* with LPS (10 pg/ml) in the presence of anti-GM-CSF blocking antibody (10 μg/ml) or isotype control (10 μg/ml). (J) Frequency of CD14$^{hi}$CD206$^+$ cells from matched donors (n = 9) in the same dataset primed with LPS and treated with anti-GM-CSF or isotype control antibody. *p* values calculated by Wilcoxon signed-rank test. LPS, lipopolysaccharide; PBMCs, peripheral blood mononuclear cells; t-SNE, t-distributed stochastic neighbour embedding.

although commonly associated with M1 polarisation, can be pro-fibrotic, a function commonly associated with M2-polarised macrophages. Future studies should also aim at determining if intrahepatic CD206$^+$ macrophages can produce HSC-activating factors such as TGFβ and PDGF.

Circulating GM-CSF concentrations were not only higher in patients with CHC and high viral load compared to healthy controls, but they were also directly correlated with other inflammatory markers such as TNFα and IL-1β, indicating that GM-CSF production is part of a broader immune activation

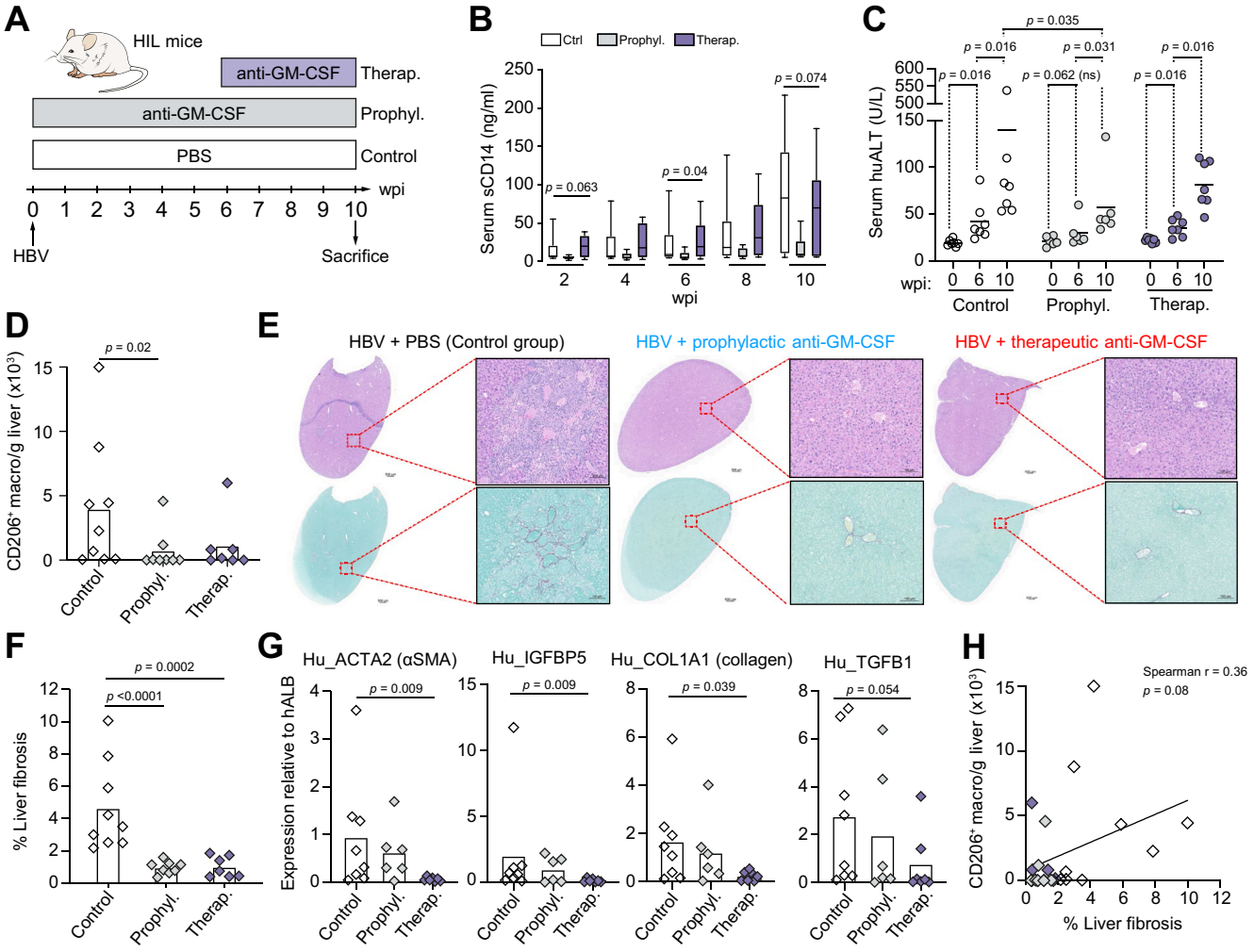


**Fig. 4. GM-CSF neutralisation inhibits intrahepatic CD206⁺ macrophage accumulation and fibrosis in viral-induced liver disease.** (A) Schedule of anti-GM-CSF antibody treatment in HBV-infected humanised mice wpi. (B) Serum sCD14 concentrations (ng/ml) in HBV-infected humanised mice untreated (n = 9) and treated with anti-GM-CSF antibody (prophylactic group, n = 8-9) followed longitudinally. (C) Measurement of human serum ALT in control (Ctrl, n = 7), prophylactic (n = 6) and therapeutic (n = 6) groups of HIL mice at 0, 6 and 10 wpi. *p* values comparing mice from the same groups or comparing groups of mice at 10 wpi were obtained using the paired Wilcoxon and the Mann-Whitney non-parametric tests, respectively. (D) Density of intrahepatic $CD14^{+}HLA\text{-}DR^{hi}CD206^{+}$ macrophages in HBV-infected mice at 10 wpi that were untreated (n = 9) or that received anti-GM-CSF antagonistic antibody at 0 wpi (prophylactic group, n = 8) or at 6 wpi (therapeutic group, n = 7) expressed as number of cells per gram of liver tissue. (E) H&E (upper panels) and Sirius Red (lower panels) staining of the liver of representative humanised mice from the 3 groups are shown. (F) % fibrosis quantification in all animals in the 3 groups. (G) Expression of human pro-fibrotic genes within HIL mouse livers at 10 wpi relative to the h*ALB* (human albumin) gene. (H) Correlation of the % liver fibrosis with numbers of intrahepatic $CD206^{+}$ macrophages (black, Ctrl; blue, prophylactic; red, therapeutic). *p* values calculated by Mann-Whitney test for (B,D,F), and by Spearman's correlation for (B). ALT, alanine aminotransferase; wpi, weeks post infection.

response. The positive correlation between circulating GM-CSF and sCD14 in HBV-infected mice suggests that this immune activation may be mediated by gut-derived bacterial products, but this remains to be directly proven in future studies. This is plausible given that chronic liver disease is associated with a breakdown of the gut barrier allowing increased translocation of bacterial products which have been shown to correlate with liver disease severity in patients[29,44–46] and promote fibrosis and HCC development.[30,31] This finding also demonstrates that GM-CSF plays a more prominent role during inflammation than during the steady state, where it is mainly required for the development of alveolar macrophages[47] and $CD103^{+}$ cDC1 in mouse non-lymphoid tissue.[48] Indeed, GM-CSF is frequently used as an adjuvant to induce the maturation of DCs to prime antigen-specific T cell responses.[9,49] This is exemplified by various treatment modalities utilising GM-CSF which are currently in clinical trials for patients with metastatic melanoma.[50,51]

Studies ascribing a proinflammatory role to GM-CSF focus on GM-CSF derived from $T_H$ cells[52] and B cells.[53] $T_H$ cells can secrete GM-CSF in response to IL-23 and IL-1[12] as well as IL-7 through STAT5 activation.[13] However, monocytes and macrophages are also potent producers of GM-CSF upon LPS stimulation.[32] In chronic viral-related liver disease, we previously showed that intrahepatic $CD14^{+}$ macrophages were the main producers of GM-CSF within pathologic livers when activated by bacterial products, while GM-CSF secretion by T cells in response to T cell receptor (TCR) engagement was modest.[2]

In this study, GM-CSF-dependent CD206$^+$ macrophage differentiation is likely due to GM-CSF generated by CD14$^+$ myeloid cells and DCs, the former being the major source. This hypothesis is corroborated by our observation of a strong correlation between the number of CD206$^+$ macrophages and GM-CSF-producing macrophages in the non-tumour liver regions of patients with HCC. In the liver of these patients, we observed a greater GM-CSF-producing capacity of CD206$^+$ macrophages compared to CD206$^-$ macrophages. This observation suggests that GM-CSF produced by CD206$^+$ macrophages could maintain their CD206$^+$ phenotype and their proinflammatory capacity in an autocrine or paracrine manner. In addition, there was no significant difference in the frequency of intrahepatic GM-CSF-producing CD206$^+$ macrophages between patients with viral- and non-viral-related HCC (Fig. S2B), suggesting that GM-CSF-mediated liver fibrosis is independent of the aetiology of chronic liver disease. It should be noted that other intrahepatic cell subsets such as mucosal-associated invariant T cells,[54] fibroblasts[55] and endothelial and epithelial cells[56] have been demonstrated to produce GM-CSF. Consistently, we also detected GM-CSF in the cytoplasm of intrahepatic CD14$^-$CK-18$^{+/-}$ non-macrophage cells but it did not correlate with CD206$^+$ macrophage accumulation. A more detailed analysis of intrahepatic GM-CSF-producing non-macrophage cells is warranted to elucidate any potential role in liver fibrosis.

The identification of GM-CSF as a potential key mediator of liver fibrosis could allow the development of targeted therapies. There are currently several clinical trials inhibiting GM-CSF or GM-CSFR using neutralising monoclonal antibodies in patients with various autoimmune diseases. The most promising candidate is mavrilimumab, a human monoclonal antibody targeting the GM-CSFR α-chain. In the recently completed phase IIb study of 326 patients with RA, mavrilimumab treatment for 24 weeks significantly reduced RA disease activity compared to placebo.[57] GSK3196165, a human monoclonal antibody which inhibits GM-CSF, showed evidence of rapid clinical responses in a phase Ib/IIa trial of 96 patients with moderate RA.[58] It is also being tested in patients with MS and a phase Ib study of 32 patients with relapsing-remitting and secondary progressive MS showed that GSK3196165 was well-tolerated but did not induce immunogenicity.[59] More recently, it has been shown that GM-CSF neutralisation with lenzilumab resulted in a reduction in neuroinflammation and cytokine release syndrome in a primary acute lymphoblastic leukaemia patient-derived xenograft model following chimeric antigen receptor T cell therapy.[60] The findings from these ongoing trials and studies will inform the use of GM-CSF-targeted therapies for the treatment of patients with chronic liver disease.

In summary, we provide evidence for a novel role of GM-CSF in liver fibrosis. We observed a strong correlation between GM-CSF, CD206$^+$ macrophages and liver fibrosis in patients with both viral and non-viral-related liver disease. Importantly, blocking GM-CSF prevented the accumulation of intrahepatic TNFα-producing CD206$^+$ macrophages and ameliorated liver fibrosis following viral-induced liver disease. These data support the use of anti-GM-CSF therapies as a novel approach for the treatment of patients with chronic liver disease.

## Abbreviations

ALT, alanine aminotransferase; BAMBI, BMP and Activin Membrane-bound Inhibitor; DAA, direct-acting antiviral; DC, dendritic cell; FFPE, formalin-fixed paraffin-embedded; GM-CSF, granulocyte-macrophage colony-stimulating factor; HCC, hepatocellular carcinoma; HIER, heat-induced epitope retrieval; HSC, hepatic stellate cells; ICS, intracellular cytokine staining; LPS, lipopolysaccharide; LSM, liver stiffness measurement; moMΦs, monocyte-derived macrophage-like cells; MS, multiple sclerosis; NASH, non-alcoholic steatohepatitis; PBMCs, peripheral blood mononuclear cells; RA, rheumatoid arthritis; SVR, sustained virological response; TCR, T cell receptor; TMA, tissue microarray; TNFα, tumour necrosis factor-α; TSA, tyramide signal amplification; t-SNE, t-distributed stochastic neighbour embedding.

## Financial support

This work was supported by the following grants - Translational and Clinical Research grant (NMRC/TCR/014-NUHS/2015) from the National Medical Research Council (NMRC), National Research Foundation Fellowship Singapore NRF-NRFF2017-03 and the Basic research New Investigator grant (NMRC/BNIG/2026/2014) from NMRC.

## Conflict of interest

The authors declare no conflicts of interest that pertain to this work.

Please refer to the accompanying ICMJE disclosure forms for further details.

## Authors' contributions

Conceptualisation: A.T-G., A.B. and C-A.D.; Experiments: A.T-G., F.L., N.P.Y., S.E.I., J.C.T.L. and C.Y.L.T.; Clinical specimens: S.P.C, T.L., R.D., E.D., R.P. and D.Y.; Animal work: F.L. and C.Q.; Data analysis: A.T-G., F.L., J.P.S.Y., R.M., N.L.B. and C-A.D.; Intellectual input: F.G.; Resources: C.Q., E.N., A.B. and C.A.D.; Writing: A.T-G., A.B. and C-A.D.

## Acknowledgments

We thank Charlene Foong Shu Fen and Pearly Yong Jean Ai from the SingHealth Flow Cytometry Core Platform for technical assistance.

## Supplementary data

Supplementary data to this article can be found online at https://doi.org/10.1016/j.jhepr.2019.11.006.

## References

[1] Fattovich G, Stroffolini T, Zagni I, Donato F. Hepatocellular carcinoma in cirrhosis: incidence and risk factors. Gastroenterology 2004;127:S35–S50.
[2] Tan-Garcia A, Wai LE, Zheng D, Ceccarello E, Jo J, Banu N, et al. Intrahepatic CD206+ macrophages contribute to inflammation in advanced viral-related liver disease. J Hepatol 2017;67:490–500.
[3] Becher B, Tugues S, Greter M. GM-CSF: from growth factor to central mediator of tissue inflammation. Immunity 2016;45:963–973.
[4] Souza LM, Boone TC, Gabrilove J, Lai PH, Zsebo KM, Murdock DC, et al. Recombinant human granulocyte colony-stimulating factor: effects on normal and leukemic myeloid cells. Science 1986;232:61–65.
[5] Touw IP. Granulocyte colony-stimulating factor and its receptor in normal myeloid cell development, leukemia and related blood cell disorders. Front Biosci 2007;12:800.
[6] Lieschke GJ, Grail D, Hodgson G, Metcalf D, Stanley E, Cheers C, et al. Mice lacking granulocyte colony-stimulating factor have chronic neutropenia, granulocyte and macrophage progenitor cell deficiency, and impaired neutrophil mobilization. Blood 1994;84:1737–1746.
[7] Dai XM, Ryan GR, Hapel AJ, Dominguez MG, Russell RG, Kapp S, et al. Targeted disruption of the mouse colony-stimulating factor 1 receptor gene results in osteopetrosis, mononuclear phagocyte deficiency, increased primitive progenitor cell frequencies, and reproductive defects. Blood 2002;99:111–120.
[8] Wiktor-Jedrzejczak W, Bartocci A, Ferrante AW, Ahmed-Ansari A, Sell KW, Pollard JW, et al. Total absence of colony-stimulating factor 1 in

the macrophage-deficient osteopetrotic (op/op) mouse. Proc Natl Acad Sci U S A 1990;87:4828–4832.
[9] Hamilton JA, Cook AD, Tak PP. Anti-colony-stimulating factor therapies for inflammatory and autoimmune diseases. Nat Rev Drug Discov 2016;16:53–70.
[10] Becher B, Spath S, Goverman J. Cytokine networks in neuroinflammation. Nat Rev Immunol 2017;17:49–59.
[11] Codarri L, Gyülvészi G, Tosevski V, Hesske L, Fontana A, Magnenat L, et al. RORγt drives production of the cytokine GM-CSF in helper T cells, which is essential for the effector phase of autoimmune neuroinflammation. Nat Immunol 2011;12:560–567.
[12] El-Behi M, Ciric B, Dai H, Yan Y, Cullimore M, Safavi F, et al. The encephalitogenicity of TH17 cells is dependent on IL-1- and IL-23-induced production of the cytokine GM-CSF. Nat Immunol 2011;12:568–575.
[13] Sheng W, Yang F, Zhou Y, Yang H, Low PY, Kemeny DM, et al. STAT5 programs a distinct subset of GM-CSF-producing T helper cells that is essential for autoimmune neuroinflammation. Cell Res 2014;24:1387–1402.
[14] Croxford AL, Lanzinger M, Hartmann FJ, Schreiner B, Mair F, Pelczar P, et al. The cytokine GM-CSF drives the inflammatory signature of CCR2+ monocytes and licenses autoimmunity. Immunity 2015;43:502–514.
[15] Yamasaki R, Lu H, Butovsky O, Ohno N, Rietsch AM, Cialic R, et al. Differential roles of microglia and monocytes in the inflamed central nervous system. J Exp Med 2014;211:1533–1549.
[16] Spath S, Komuczki J, Hermann M, Pelczar P, Mair F, Schreiner B, et al. Dysregulation of the cytokine GM-CSF induces spontaneous phagocyte invasion and immunopathology in the central nervous system. Immunity 2017;46:245–260.
[17] Carrieri PB, Provitera V, De Rosa T, Tartaglia G, Gorga F, Perrella O. Profile of cerebrospinal fluid and serum cytokines in patients with relapsing-remitting multiple sclerosis: a correlation with clinical activity. Immunopharmacol Immunotoxicol 1998;20:373–382.
[18] Bell AL, Magill MK, McKane WR, Kirk F, Irvine AE. Measurement of colony-stimulating factors in synovial fluid: potential clinical value. Rheumatol Int 1995;14:177–182.
[19] Pereira J, Velloso ED, Loterio HA, Laurindo IM, Chamone DA. Long-term remission of neutropenia in Felty's syndrome after a short GM-CSF treatment. Acta Haematologica 1994;92:154–156.
[20] Lakhani S, Ellis I, Schnitt S, Tan P, Van de Vijver M. World Health Organisation Classification of Tumors of the Breast. 2012.
[21] Ishak K, Baptista A, Bianchi L, Callea F, De Groote J, Gudat F, et al. Histological grading and staging of chronic hepatitis. J Hepatol 1995;22:696–699.
[22] Goodman ZD. Grading and staging systems for inflammation and fibrosis in chronic liver diseases. J Hepatol 2007;47:598–607.
[23] Thike AA, Yong-Zheng Chong L, Cheok PY, Li HH, Wai-Cheong Yip G, Huat Bay B, et al. Loss of androgen receptor expression predicts early recurrence in triple-negative and basal-like breast cancer. Mod Pathol 2013;27:352–360.
[24] Dutertre CA, Amraoui S, DeRosa A, Jourdain JP, Vimeux L, Goguet M, et al. Pivotal role of M-DC8(+) monocytes from viremic HIV-infected patients in TNFalpha overproduction in response to microbial products. Blood 2012;120:2259–2268.
[25] Guilliams M, Dutertre CA, Scott CL, McGovern N, Sichien D, Chakarov S, et al. Unsupervised high-dimensional analysis aligns dendritic cells across tissues and species. Immunity 2016;45:669–684.
[26] Keng CT, Sze CW, Zheng D, Zheng Z, Yong KS, Tan SQ, et al. Characterisation of liver pathogenesis, human immune responses and drug testing in a humanised mouse model of HCV infection. Gut 2015. https://doi.org/10.1136/gutjnl-2014-307856.
[27] Bajaj JS, Sterling RK, Betrapally NS, Nixon DE, Fuchs M, Daita K, et al. HCV eradication does not impact gut dysbiosis or systemic inflammation in cirrhotic patients. Aliment Pharmacol Ther 2016;44:638–643.
[28] Negash AA, Ramos HJ, Crochet N, Lau DTY, Doehle B, Papic N, et al. IL-1β production through the NLRP3 inflammasome by hepatic macrophages links hepatitis C virus infection with liver inflammation and disease. PLoS Pathog 2013;9:1–13.
[29] Sandler NG, Koh C, Roque A, Eccleston JL, Siegel RB, Demino M, et al. Host response to translocated microbial products predicts outcomes of patients with HBV or HCV infection. Gastroenterology 2011;141:1220–1230.e3.
[30] Dapito DH, Mencin A, Gwak GY, Pradere JP, Jang MK, Mederacke I, et al. Promotion of hepatocellular carcinoma by the intestinal microbiota and TLR4. Cancer Cell 2012;21:504–516.
[31] Seki E, De Minicis S, Österreicher CH, Kluwe J, Osawa Y, Brenner DA, et al. TLR4 enhances TGF-β signaling and hepatic fibrosis. Nat Med 2007;13:1324–1332.
[32] Hamilton JA. Coordinate and noncoordinate colony stimulating factor formation by human monocytes. J Leukoc Biol 1994;55:355–361.
[33] Däbritz J, Weinhage T, Varga G, Wirth T, Walscheid K, Brockhausen A, et al. Reprogramming of monocytes by GM-CSF contributes to regulatory immune functions during intestinal inflammation. J Immunol 2015;194:2424–2438.
[34] Kittan NA, Allen RM, Dhaliwal A, Cavassani KA, Schaller M, Gallagher KA, et al. Cytokine induced phenotypic and epigenetic signatures are key to establishing specific macrophage phenotypes. PLoS One 2013;8:1–15.
[35] Neu C, Sedlag A, Bayer C, Forster S, Crauwels P, Niess JH, et al. CD14-Dependent monocyte isolation enhances phagocytosis of Listeria monocytogenes by proinflammatory, GM-CSF-derived macrophages. PLoS One 2013;8.
[36] Mills CD, Kincaid K, Alt JM, Heilman MJ, Hill AM. M-1/M-2 macrophages and the Th1/Th2 paradigm. J Immunol 2000;164:6166–6173.
[37] Stein M, Keshav S, Harris N, Gordon S. Interleukin 4 potently enhances murine macrophage mannose receptor activity: a marker of alternative immunologic macrophage activation. J Exp Med 1992;176:287–292.
[38] Ginhoux F, Schultze JL, Murray PJ, Ochando J, Biswas SK. New insights into the multidimensional concept of macrophage ontogeny, activation and function. Nat Immunol 2016;17:34–40.
[39] Tacke F, Zimmermann HW. Macrophage heterogeneity in liver injury and fibrosis. J Hepatol 2014;60:1090–1096.
[40] Pradere JP, Kluwe J, De Minicis S, Jiao JJ, Gwak GY, Dapito DH, et al. Hepatic macrophages but not dendritic cells contribute to liver fibrosis by promoting the survival of activated hepatic stellate cells in mice. Hepatology 2013;58:1461–1473.
[41] Osawa Y, Hoshi M, Yasuda I, Saibara T, Moriwaki H, Kozawa O. Tumor necrosis factor-α promotes cholestasis-induced liver fibrosis in the mouse through tissue inhibitor of metalloproteinase-1 production in hepatic stellate cells. PLoS One 2013;8:1–10.
[42] Liu C, Chen X, Yang L, Kisseleva T, Brenner DA, Seki E. Transcriptional repression of the transforming growth factor β (TGF-β) pseudoreceptor BMP and activin membrane-bound inhibitor (BAMBI) by nuclear factor κB (NF-κB) p50 enhances TGF-β signaling in hepatic stellate cells. J Biol Chem 2014;289:7082–7091.
[43] Tomita K, Tamiya G, Ando S, Ohsumi K, Chiyo T, Mizutani A, et al. Tumour necrosis factor α signalling through activation of Kupffer cells plays an essential role in liver fibrosis of non-alcoholic steatohepatitis in mice. Gut 2006;55:415–424.
[44] Lin RS, Lee FY, Lee SD, Tsai YT, Lin HC, Lu RH, et al. Endotoxemia in patients with chronic liver diseases: relationship to severity of liver diseases, presence of esophageal varices, and hyperdynamic circulation. J Hepatol 1995;22:165–172.
[45] Chan CC, Hwang SJ, Lee FY, Wang SS, Chang FY, Li CP, et al. Prognostic value of plasma endotoxin levels in patients with cirrhosis. Scand J Gastroenterol 1997;32:942–946.
[46] Wiest R, Lawson M, Geuking M. Pathological bacterial translocation in liver cirrhosis. J Hepatol 2014;60:197–209.
[47] Guilliams M, De Kleer I, Henri S, Post S, Vanhoutte L, De Prijck S, et al. Alveolar macrophages develop from fetal monocytes that differentiate into long-lived cells in the first week of life via GM-CSF. J Exp Med 2013;210:1977–1992.
[48] Greter M, Helft J, Chow A, Hashimoto D, Mortha A, Agudo-Cantero J, et al. GM-CSF controls nonlymphoid tissue dendritic cell homeostasis but is dispensable for the differentiation of inflammatory dendritic cells. Immunity 2012;36:1031–1046.
[49] Van De Laar L, Coffer PJ, Woltman AM. Regulation of dendritic cell development by GM-CSF: molecular control and implications for immune homeostasis and therapy. Blood 2012;119:3383–3393.
[50] Andtbacka RHI, Kaufman HL, Collichio F, Amatruda T, Senzer N, Chesney J, et al. Talimogene laherparepvec improves durable response rate in patients with advanced melanoma. J Clin Oncol 2015;33:2780–2788.
[51] Hodi FS, Lee S, McDermott DF, Rao UN, Butterfield LH, Tarhini AA, et al. Ipilimumab plus sargramostim vs ipilimumab alone for treatment of metastatic melanoma: a randomized clinical trial. Jama 2014;312:1744–1753.
[52] Croxford AL, Spath S, Becher B. GM-CSF in neuroinflammation: licensing myeloid cells for tissue damage. Trends Immunol 2015;36:651–662.

[53] Li R, Rezk A, Miyazaki Y, Hilgenberg E, Touil H, Shen P, et al. Proinflammatory GM-CSF-producing B cells in multiple sclerosis and B cell depletion therapy. Sci Translational Med 2015;7:310ra166.
[54] Meierovics AI, Cowley SC. MAIT cells promote inflammatory monocyte differentiation into dendritic cells during pulmonary intracellular infection. J Exp Med 2016:2793–2809.
[55] Anzai A, Choi JL, He S, Fenn AM, Nairz M, Rattik S, et al. The infarcted myocardium solicits GM-CSF for the detrimental oversupply of inflammatory leukocytes. J Exp Med 2017:20170689.
[56] Hamilton JA. GM-CSF in inflammation and autoimmunity. Trends Immunol 2002;23:403–408.
[57] Burmester GR, McInnes IB, Kremer JM, Miranda P, Korkosz M, Vencovsky J, et al. A randomised phase IIb study of mavrilimumab, a novel GM–CSF receptor alpha monoclonal antibody, in the treatment of rheumatoid arthritis. Ann Rheum Dis 2017:1–11.
[58] Behrens F, Tak PP, Østergaard M, Stoilov R, Wiland P, Huizinga TW, et al. MOR103, a human monoclonal antibody to granulocyte–macrophage colony-stimulating factor, in the treatment of patients with moderate rheumatoid arthritis: results of a phase Ib/IIa randomised, double-blind, placebo-controlled, dose-escalation trial. Ann Rheum Dis 2015;74:1058–1064.
[59] Constantinescu CS, Asher A, Fryze W, Kozubski W, Wagner F, Aram J, et al. Randomized phase 1b trial of MOR103, a human antibody to GM-CSF, in multiple sclerosis. Neurol Neuroimmunol Neuroinflamm 2015;2:1–9.
[60] Sterner RM, Sakemura R, Cox MJ, Yang N, Khadka RH, Forsman CL, et al. GM-CSF inhibition reduces cytokine release syndrome and neuroinflammation but enhances CAR-T cell function in xenografts. Blood 2019;133:697–709.